Brain, Behavior, and Immunity 136 (2026) 106539

Contents lists available at ScienceDirect

Brain Behavior and Immunity

journal homepage: www.elsevier.com/locate/ybrbi

Full-length Article

Impact of voluntary exercise on obesity-induced brain pathology: Insights from a multimodal approach in male Ldlr-/-.Leiden mice

Xiaoxue Liang [a], Klara J. Lohkamp [a], Anita M. van den Hoek [b], Bram Geenen [a], Vivienne Verweij [a], Martine C. Morrison [b], Robert Kleemann [b], Amanda J. Kiliaan [a,*], Maximilian Wiesmann [a,1], Gemma Solé-Guardia [a,c,1]

[a] Department of Medical Imaging, Anatomy, Research Institute for Medical Innovation, Radboud University Medical Center, Donders Institute for Brain, Cognition and Behavior, Center for Medical Neuroscience, Radboud Technology Center Preclinical imaging PRIME, Radboud Alzheimer Center, Nijmegen, the Netherlands
[b] Department of Metabolic Health Research, The Netherlands Organization for Applied Scientific Research (TNO), Leiden, the Netherlands
[c] Department of Neurology, Research Institute for Medical Innovation, Radboud University Medical Center, Donders Institute for Brain, Cognition and Behavior, Center for Medical Neuroscience, Nijmegen, the Netherlands

ARTICLE INFO

Keywords:
Obesity
Voluntary exercise
Microvasculature
Microgliosis
Astrogliosis
Axonal injury
Myelin integrity
MRI

ABSTRACT

Background: Impact of exercise on obesity-related brain pathology remains unclear. MRI is used to detect obesity-related brain changes, but its interpretation remains unclear. We aimed to evaluate effects of voluntary exercise on obesity-induced brain pathology and determine whether MRI signal intensity and diffusion metrics capture these alterations.

Methods: Male Ldlr-/-.Leiden mice were fed a low-fat chow diet from 2 to 4 months of age. At 4 months, mice (n = 10) were sacrificed as baseline group representing young non-obese adult mouse brains. Remaining mice were fed a high-fat diet (HFD) for another 6 months with (HFD + exercise) or without (HFD) access to running wheels (n = 16/group each). MRI (T1-weighted, T2-weighted, T2*-weighted, and diffusion metrics) was analyzed for signal intensity and microstructural changes, rather than visible cerebral small vessel disease lesions. Immunohistochemistry (IHC), polarized light imaging (PLI), and qPCR were used to investigate microvasculature, astro-/microgliosis, and axonal/myelin integrity. We studied MRI's underlying pathology by its co-registration with IHC and PLI.

Results: HFD induced microvascular remodeling, astro-/microgliosis, and axonal injury, while myelin integrity remained unaffected. Exercise did not fully reverse these changes but was associated with milder microgliosis, microvascular remodeling and axonal alterations. MRI revealed reduced T2-weighted signal intensity in white matter (WM) (HFD), and in both WM and grey matter (GM) (HFD + exercise). Additionally, GM microglial density correlated negatively with diffusion metrics in the HFD + exercise group.

Conclusion: Voluntary exercise offered partial mitigation of HFD-induced damage, with indications of less severe microgliosis, microvascular remodeling and axonal disruption. Pathology-MRI co-registration revealed

Abbreviations: AD, axial diffusivity; AU, arbitrary units; ADC, apparent diffusion coefficient; ANOVA, multivariate analysis of variance; BBB, Blood-brain barrier; BMI, body-mass index; BSA, bovine serum albumin; B2M, beta-2 microglobulin; CBF, cerebral blood flow; cSVD, cerebral small vessel disease; CSF, cerebrospinal fluid; Ct, threshold cycle; CT, cortex; DAB-Ni, 3,3′-diaminobenzidine-nickel; DAPI, 4′,6-diamidino-2-phenylindole; DTI, diffusion tensor imaging; DWI, diffusion-weighted imaging; FA, fractional anisotropy; GAPDH, glyceraldehyde-3-phosphate dehydrogenase; GFAP, glial fibrillary acidic protein; GLUT-1, glucose transporter-1; GM, grey matter; HFD, high-fat diet; HIP, hippocampus; IHC, immunohistochemistry; IBA-1, ionized calcium-binding adapter molecule-1; Ldlr-/-. Leiden, low-density lipoprotein receptor knock-out Leiden; MRI, magnetic resonance imaging; MD, mean diffusivity; NfL, neurofilament light chain protein; OCCL, occluding; PBS, phosphate-buffered saline; PLI, polarized light imaging; PRIME, Radboud Technology Center Preclinical imaging; qPCR, quantitative polymerase chain reaction; RD, radial diffusivity; ROI, regions of interest; SEM, standard error of mean; TH, thalamus; WM, white matter; WMH, white matter hyperintensities; ZO-1, zonula occludens-1.

* Corresponding author.
E-mail addresses: Xiaoxue.Liang@radboudumc.nl (X. Liang), Klara.Lohkamp@radboudumc.nl (K.J. Lohkamp), a.vandenhoek@tno.nl (A.M. van den Hoek), Bram.Geenen@radboudumc.nl (B. Geenen), Vivienne.Verweij@radboudumc.nl (V. Verweij), Martine.Morrison@tno.nl (M.C. Morrison), Robert.Kleemann@tno.nl (R. Kleemann), Amanda.Kiliaan@radboudumc.nl (A.J. Kiliaan), Maximilian.Wiesmann@radboudumc.nl (M. Wiesmann), Gemma.SoleGuardia@radboudumc.nl (G. Solé-Guardia).
[1] These authors contributed equally.

https://doi.org/10.1016/j.bbi.2026.106539
Received 25 September 2025; Received in revised form 5 March 2026; Accepted 11 March 2026
Available online 17 March 2026

associations between neuroinflammation and diffusion metrics, supporting multimodal approaches to interpret MRI and guide development of optimal targeted interventions for obesity-related brain pathology.

1. Introduction

Obesity, defined as a body mass index (BMI) ≥ 30, is a major global health challenge accounting for approximately 4 million deaths and 120 million disability-adjusted life-years worldwide (Afshin et al., 2017). By 2035, more than half of the world's population is expected to be either overweight or obese (Martin et al., 2024). As obesity prevalence continues to rise, obesity-related health issues, such as neurodegenerative disorders, are also expected to increase (Elzinga et al., 2025; Lv et al., 2025; Martin et al., 2024; Worrall and Thohan, 2024). Although many studies have pointed out that obesity is associated with brain dysfunction, the underlying mechanisms still need further clarification.

Accumulating evidence suggests that obesity may affect brain function through cerebral small vessel disease (cSVD) (Marini et al., 2020). cSVD is the most common form of cerebrovascular diseases and a major contributor to cognitive decline and dementia (Anderson et al., 2024; Evans et al., 2021). On magnetic resonance imaging (MRI), cSVD typical markers include white matter hyperintensities (WMH), lacunes, among others (Duering et al., 2023). However, these are hypothesized to reflect relatively advanced stages of disease. Therefore, our study focuses on early indicators of brain pathology preceding overt cSVD markers. We examine MRI signal intensity (T1-weighted, T2-weighted, T2*-weighted) and diffusion metrics, suggested to capture underlying (microstructural) changes (Maillard et al., 2013; Solé-Guardia et al., 2025), and their association with obesity-related brain pathology. For instance, T2-weighted signal is sensitive to microstructural changes, such as white matter damage, in humans (Solé-Guardia et al., 2025). Mechanistically, obesity is associated with a cascade of blood-brain barrier (BBB) dysfunction, decreased cerebral blood flow (CBF), and neuroinflammation, processes central to the pathogenesis of cSVD (Bailey et al., 2011; Low et al., 2020). BBB integrity depends on the structure and function of the neurovascular unit composed of neurons, astrocytes, microglia, pericytes, endothelial cells, and extracellular matrix (Feng et al., 2024; Muoio et al., 2014). Obesity often coexists with vascular comorbidities like hypertension and atherosclerosis, further exacerbating neurovascular dysfunction and increasing cSVD risk (Masi et al., 2021). Together, these likely act cumulatively to disrupt the neurovascular unit, leading to BBB dysfunction and neuroinflammation (Evans et al., 2021; Feng et al., 2024). Exercise may improve obesity and brain alterations (Blair and Church, 2004; Colcombe et al., 2003) likely by promoting vascular health, improving CBF, and reducing neuroinflammation (Lucas et al., 2015; Mahalakshmi et al., 2020), thereby potentially mitigating cSVD-related pathology. Animal models provide a unique experimental framework to disentangle the impact of exercise on obesity- and cSVD-related brain pathology (Lohkamp et al., 2023). The low-density lipoprotein receptor knock-out Leiden (Ldlr-/-.Leiden) mouse is a highly translational model of obesity and metabolic dysfunction recapitulating key vascular and metabolic complications akin to humans at a molecular level (Seidel et al., 2023). On a high-fat diet (HFD), this model exhibits hypertension, white adipose tissue inflammation, insulin resistance, dyslipidemia, and atherosclerosis (Morrison et al., 2018; Olga et al., 2022; Seidel et al., 2022; van den Hoek et al., 2020). As a result, this model shows similar cSVD-related alterations as observed in humans such as endothelial dysfunction, BBB leakage, impaired CBF, neuroinflammation, white matter loss, and impaired spatial memory (Arnoldussen et al., 2022; Arnoldussen et al., 2017; Jia et al., 2025; Lohkamp et al., 2023; Seidel et al., 2023; Seidel et al., 2025).

Therefore, the HFD-fed Ldlr-/-.Leiden mice provide a unique opportunity to further elucidate obesity-related cSVD brain pathology and the potential neuroprotective effects of exercise. As previous studies have examined obesity-related brain changes using either imaging or histology separately (Feng et al., 2024; Le Thuc and Garcia-Caceres, 2024; Tanaka et al., 2020), a combined analysis of imaging and pathology in the Ldlr-/-.Leiden mouse model will further help to reveal underlying pathological alterations in early MRI markers. This study aimed (1) to evaluate the effect of voluntary exercise on obesity-induced brain pathology and (2) to determine whether MRI signal intensity and diffusion metrics reflect these pathological alterations.

2. Materials and methods

2.1. Animals, diets, and study design

This animal study was approved by the Central Authority for Scientific Procedures on Animals (CCD, The Hague, the Netherlands, approval number: AVD5010020172064). Ethical approval was provided by the TNO Animal Welfare Body (TNO, the Netherlands; Permit number: TNO-476) and the Veterinary Authority of the Radboud university medical center (Nijmegen, the Netherlands; approval number: 2020-0033-001). This study was conducted and reported following ARRIVE guidelines (Percie du Sert et al., 2020).

This study used male Ldlr-/-.Leiden mice under HFD feeding (Jia et al., 2025; Morrison et al., 2018; Olga et al., 2022; Seidel et al., 2025; van den Hoek et al., 2020) to evaluate the effects of voluntary exercise on obesity-related brain changes and the correlation between imaging and pathological changes. Male mice were selected because they exhibit greater susceptibility to metabolic disorders compared to females and are not subject to variability related to the estrous cycle (Seguella et al., 2025). Female mice will be included in future studies to investigate potential sex-specific effects. A total of 48 male Ldlr-/-.Leiden mice were used in this study. At 2 months of age ($t = -2$), 6 mice were excluded from this study due to showing very low glucose levels after 5h of fasting. Low glucose levels may indicate abnormal liver function and increased susceptibility to fibrosis (Lohkamp et al., 2023). Finally, 42 male Ldlr-/-.Leiden mice were transferred from a specified pathogen-free breeding stock at the AAALAC-accredited animal facility at TNO Metabolic Health Research (Leiden, the Netherlands) to the Radboud Technology Center Preclinical imaging PRIME at the Animal Research Facility at Radboudumc (Nijmegen, the Netherlands).

Sample size was based on previous studies using the Ldlr-/-.Leiden model to detect diet-induced neuroinflammatory changes with similar outcome measures (Lohkamp et al., 2023). Throughout the entire experiment, mice on the same diet were housed in pairs in digitally ventilated cages (DVC; Tecniplast SPA, Buguggiate (VA) Italy) with a relative humidity of 50–60%, temperature of 21 °C, light cycle of 7 a.m.–7 p.m., and ad libitum access to food and autoclaved water.

The detailed study design is shown in Fig. 1. From 2 months to 4 months of age (from $t = -2$ to $t = 0$), all mice were fed a conventional low-fat chow diet (chow, Sniff R/M-H diet V1534-703, Sniff Spezialdiäten GmbH, Soest, Germany). At 4 months of age ($t = 0$), after MRI scanning, 10 mice were sacrificed by transcardial perfusion and served as a baseline group. Their brains were collected for IHC, PLI, and quantitative polymerase chain reaction (qPCR) analysis. The baseline group provided a physiological reference prior to dietary and exercise interventions and represented young non-obese adult brains. The remaining mice were matched based on body weight and metabolic parameters (blood glucose, plasma cholesterol, and plasma triglyceride levels). Within each matched pair, mice were randomized across the two experimental groups, ensuring balanced groups using a computer-generated randomization procedure. Investigators performing MRI acquisition, histological processing, and quantitative analysis were

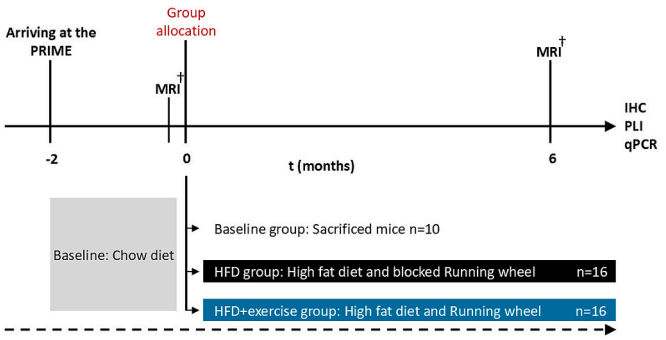

Fig. 1. Study design. At 2 months (t = −2), 42 male Ldlr-/-.Leiden mice were housed in pairs. All mice were fed a conventional low-fat chow diet for 2 months. At 4 months (t = 0), 10 mice underwent magnetic resonance imaging (MRI) and were sacrificed as baseline group. Brains were processed for immunohistochemistry (IHC), polarized light imaging (PLI), and quantitative polymerase chain reaction (qPCR). Remaining mice were matched for metabolic parameters into 2 groups. (1) High-fat diet (HFD; n = 16): HFD with blocked running wheel. (2) HFD+exercise (n = 16): HFD with running wheel. At 10 months (t = 6), both groups underwent MRI and were sacrificed (†) by transcardial perfusion for IHC, PLI, and qPCR.

blinded to group allocation until completion of data analysis. The first group (HFD, n = 16) was fed a high-fat diet (HFD; D12451 Research Diets, New Brunswick, NJ, USA, 46.0% kcal fat, 36.0% carbohydrate, and 18.0% kcal protein) for another 6 months and was equipped with a blocked functional running wheel (GYM500 activity wheel, Tecniplast S. p.A., Buguggiate (VA), Italy) in their home cage. The second group (HFD+exercise, n = 16) was also kept on HFD for another 6 months with access to a functional running wheel in their home cage 24/7. The Supplementary Table S1 shows a detailed composition of the HFD. A total of 2 mice from the HFD group were excluded from the analysis: 1 mouse was sacrificed before the end of the experiment due to hind paw paralysis, and 1 mouse did not complete the MRI examination. Six months after allocation (t = 6), mice in the HFD group (n = 14) and HFD+exercise group (n = 16) were sacrificed after completing the MRI scan, and their brains were collected for IHC, PLI, and qPCR analysis. The Supplementary Table S2 and S3 shows a detailed sample size and the reason for exclusion. The Supplementary Table S4 shows average body weight, food intake, systolic blood pressure, and plasma markers per group.

Home-cage activity of pair-housed mice was monitored 24/7 in DVC (Iannello, 2019). Mouse movements across the cage was detected through a capacitive sensing board including 12 capacitive-based electrodes, placed under each DVC, that measured changes in electrical capacitance (Iannello, 2019). Activity was determined as the absolute difference in capacitance between consecutive measurements every 250 ms. Given the positioning of the blocked running wheel (above electrode 6), the final analysis consists of the average activity from the other 11 electrodes for 12-hour day and night periods. To reduce sources of activity disruption, such as experiments and cage cleaning, only weekend home-cage activity data was used. Activity was normalized by the number of mice per cage (n = 2). Average activity per mouse and distance per mouse in HFD+exercise group is shown in Supplementary Table S5.

2.2. Magnetic resonance imaging (MRI) protocol

MRI of the whole mouse brain was performed on an 11.7T BioSpec Avance III small animal MR system (Bruker Biospin, Ettlingen, Germany) interfaced with an actively shielded gradient set of 600 mT/m and processed on Paravision 6.0.1 software (Bruker, Karlsruhe, Germany). The baseline group was imaged before allocation (t = 0). HFD and HFD+exercise groups were imaged at 6 months after allocation (t = 6). To ensure comparable imaging parameters across different mice, we established identical imaging scanning and processing conditions for all mice.

Before MRI scanning, mice were fully anesthetized using isoflurane (induction: 3.5%, maintenance: 1.8%; Abbott Animal Health, Abbot Park, IL, USA). The head of the mouse was placed in a stereotactic holder for fixation. Throughout scanning, respiration and body temperature were monitored with a pneumatic cushion respiratory monitoring system (Small Animal Instruments Inc., Stony Brook, New York, NY, USA) and a rectal thermometer, respectively. The body temperature was maintained at 37℃ by using a water heating pad. Detailed MRI parameters are shown in Supplementary Table S6.

2.3. Magnetic resonance imaging (MRI) processing

T1-weighted, T2-weighted, T2*-weighted, diffusion tensor imaging (DTI), diffusion-weighted imaging (DWI), and apparent diffusion coefficient (ADC) images were extracted using the medical imaging toolbox MP3 in Matlab R2020a (version 9.8.0.1873465, 64 bit, MathWorks, Natick, MA, USA) (Brossard et al., 2020).

T1-weighted, T2-weighted and T2*-weighted imaging signal intensities were used as indicators of underlying changes associated with obesity-related brain pathology. DWI, ADC, and DTI were used to evaluate the white matter (WM) and grey matter (GM) microstructural integrity (Defrancesco et al., 2014; Wiesmann et al., 2017). We examined mean diffusivity (MD), fractional anisotropy (FA), axial diffusivity (AD), and radial diffusivity (RD) derived from DTI. MD is the average water diffusivity in tissue regardless of the direction of diffusion (Bennett and Madden, 2014). AD is the water diffusivity along the main diffusion direction, and RD represents diffusivity perpendicular to the main diffusion direction (Behler et al., 2023; Kaushal et al., 2019). FA represents the anisotropy of water diffusion regardless of diffusivity, and higher FA reflects water diffusion in a certain direction (Bennett and Madden, 2014).

Coronal images covering the whole brain and close to bregma -1.94 were selected for quantification by manually delineating 6 regions of interest (ROIs), including cortex, hippocampus, thalamus, corpus callosum, fimbria, and external capsule. ROIs were drawn using ImageJ (ImageJ 1.53t, National Institutes of Health, USA) according to the atlas of Franklin and Paxinos (Franklin and Paxinos, 2019). FA, MD, RD, and AD were calculated as reported previously (Zerbi et al., 2013).

2.4. Tissue preparation

After MRI scanning, mice were sacrificed by transcardial perfusion with phosphate-buffered saline (PBS). Brains were collected and divided into left and right cerebral hemispheres. The cortex, thalamus, and hippocampus were dissected from the right cerebral hemisphere and rapidly frozen in liquid nitrogen for qPCR. Data shown in Supplementary Materials and Methods. The left cerebral hemisphere was fixed in 4% paraformaldehyde at 4℃ for 24 hours, then transferred to 0.1 M PBS containing 0.01% sodium azide, and stored at 4℃ until sectioning. Before sectioning, the brain tissue was placed in 0.1 M PBS containing 30% sucrose at room temperature overnight for cryoprotection. The left cerebral hemisphere was cut into 30 μm free-floating coronal sections using a sliding microtome (Microm HC 440, Walldorf, Germany). A total of 8 serial free-floating left coronal sections were obtained and used for IHC and PLI.

2.5. Immunohistochemistry (IHC)

We performed four 3,3'-diaminobenzidine-nickel (DAB-Ni) IHC using a previously described standardized protocol (see Table 1 for detailed information on used antibodies) (Janssen et al., 2016). First, Glucose transporter-1 (GLUT-1), a marker mainly expressed in microvascular endothelial cells, was used to assess microvascular integrity

Table 1
Primary and secondary antibody information for IHC.

Antibody name	Antibody type	Dilution ratio	Manufacturer	RRID
Primary antibody	Polyclonal rabbit anti-GLUT-1	1:40000	Millipore, Burlington, MA, USA	AB_11212210
	Polyclonal goat anti-IBA-1	1:4000	Abcam, Cambridge, UK, Europe	AB_2340397
	Polyclonal rabbit anti-GFAP	1:80000	AKO, Santa Clara, California, USA	AB_10013382
	Monoclonal rabbit anti-NfL	1:30000	Abcam, Cambridge, UK, Europe	AB_2891198
	Monoclonal rabbit anti-ZO-1	1:2000	Abcam, Cambridge, UK, Europe	AB_2892660
Secondary antibody	Donkey anti-goat biotin	1:1500	Jackson Immunoresearch, Cambridgeshire, UK, Europe	AB_2340397
	Donkey anti-rabbit biotin	1:1500	Thermo Scientific, Waltham, MA, USA	AB_228212

(Winkler et al., 2015). Second, ionized calcium-binding adapter molecule-1 (IBA-1), a microglia/macrophage-specific marker, was used to evaluate microglial activation and neuroinflammation (Wang et al., 2018). Third, glial fibrillary acidic protein (GFAP), mainly expressed in astrocytes, was used as an indicator of astrocytes activation and neuroinflammation(Azzolini et al., 2022). Fourth, neurofilament light chain protein (NfL), a neuron-specific cytoskeletal component, was used to assess neuroaxonal damage (Abu-Rumeileh et al., 2023). Briefly, free-floating coronal sections were pre-incubated in blocking solution (3% bovine serum albumin (BSA) and 0.5% Triton X-100 in PBS) for 30 minutes and then incubated with primary antibodies (see Table 1) overnight at room temperature to reduce nonspecific background. Afterward, a series of free-floating sections were incubated with secondary antibodies (Table 1) at room temperature for 1.5 hours. The sections were visualized by incubating in DAB-Ni solution (Sigma-Aldrich, Burlington, Massachusetts, United States), then mounted on gelatin-coated slides. After overnight drying, the slides were dehydrated, cover-slipped with Entellan (Merck, Darmstadt, Germany), and examined under a light microscope.

We performed fluorescent IHC for zonula occludens-1 (ZO-1), tight junction protein in endothelial cells, that reflects the tight junction integrity between endothelial cells (Tornavaca et al., 2015). Free-floating coronal sections were pre-incubated in blocking solution (3% BSA and 0.5% Triton X-100 in PBS) for 30 minutes and then separately incubated with primary antibodies (see Table 1) overnight at room temperature. Subsequently, a series of free-floating sections were incubated with secondary antibodies (see Table 1) at room temperature for 3 hours. Free-floating sections were mounted on gelatin-coated slides which then dried at room temperature in the dark. After 30 minutes, the slides were covered with Fluormount-G with DAPI (1:1000, Thermo Fisher Scientific, Waltham, MA, USA), and dried at room temperature overnight in the dark. The signal was observed by a fluorescence microscope.

2.6. Polarized light imaging (PLI)

PLI was used to evaluate the orientation and density of myelin, based on its birefringent properties (Mollink et al., 2019; Mollink et al., 2017). For PLI, 30 μm thick coronal sections were mounted on uncoated glass slides and dried at 37 ℃ for 24 hours. Afterwards, the slides were covered with polyvinylpyrrolidone (Sigma-Aldrich, Burlington, Massachusetts, United States) mounting medium and then dried for at least 1 week. The detailed procedure for PLI processing and setup has been documented in a previously published study (Lohkamp et al., 2023). We obtained the following PLI outcomes: dispersion as an indicator of myelin orientation and retardance as an indicator of myelin density.

2.7. Quantification of IHC and PLI

All IHC and PLI sections were digitized (Aperio AT2, Leica Biosystems, Amsterdam, The Netherlands). Brain sections close to bregma -1.94 were selected for quantification, and were used to manually delineate 6 ROIs across WM and GM, including cortex, hippocampus, thalamus, corpus callosum, fimbria, and external capsule, using polygon selection tool in ImageJ according to the atlas of Franklin and Paxinos (Franklin and Paxinos, 2019).

Quantitative analysis was performed using ImageJ. Firstly, both IHC and PLI sections were converted to 8-bit greyscale (0-255), and then we applied an intensity threshold to separate positive staining from background. Threshold settings were established per staining. For GLUT-1, IBA-1, GFAP, and NfL stainings, mean greyscale values were inverted (255 – mean intensity) to generate an intensity index proportional to the amount of staining signal, where higher values indicate greater staining signal. Because mean greyscale values for ZO-1 were already proportional to staining intensity, ZO-1 intensity values were not inverted. The final intensity value was expressed in arbitrary units (AU). For all stainings, the relative area was calculated as the percentage of the ROI occupied by positive staining. GLUT-1 microvascular density was defined as the number of GLUT-1 positive (GLUT-1+) microvessels per mm^2. ZO-1 microvascular density was defined using an equivalent procedure. In addition, average vessel size was calculated for individual ZO-1+ vessels. For IBA-1, we also evaluated the average size of IBA-1+ cells, the IBA-1+ cellular density, and their circularity. Cellular density was expressed as the number of IBA-1+ cells per mm^2. Circularity (range 0–1) was derived following segmentation, where higher circularity values indicate a more rounded/amoeboid morphology (Elsaafien et al., 2023).

Myelin orientation (dispersion) and myelin density (retardance) derived from PLI were quantitatively analyzed using ImageJ. PLI dispersion values were calculated by inverting mean intensity values (255 – mean intensity), whereas PLI retardance values were obtained directly. Higher values in dispersion may serve as an indirect measure for greater myelin microstructural integrity, and lower values in retardance may serve as a marker for myelin loss (Mollink et al., 2019). Final intensity values were expressed in AU.

2.8. Pathology-MRI co-registration and regions of interest (ROI)

Prior to pathology-MRI co-registration, all IHC sections were registered based on manually selected anatomical landmarks, with GFAP section as a reference. Co-registration results among all IHC sections were thoroughly checked to ensure robustness. PLI sections were then registered to the IHC sections using the same method. Co-registration was performed using the "Align Image by line ROI" plugin in ImageJ (Schindelin et al., 2012), by selecting two consistent reference points in all images and connecting them with a straight line. Subsequently, MRI were registered to the IHC and PLI section using the same procedure. Following affine transformation-based registration, we manually checked that all images were correctly co-registered.

After Pathology-MRI co-registration, we manually segmented the abovementioned 6 ROIs (bregma -1.94: cortex, hippocampus, thalamus, corpus callosum, external capsule, fimbria) using ImageJ, according to the Atlas of Franklin and Paxinos (Franklin and Paxinos, 2019). While these ROIs were used to derive the abovementioned IHC, PLI and MRI outcomes (e.g. intensity), results for statistical analysis are shown as WM, comprising the corpus callosum, external capsule, and fimbria; and GM, comprising the cortex, hippocampus, and thalamus. Intensity values were expressed in AU.

2.9. Statistics

Data analysis was conducted using IBM SPSS Statistics 29 (IBM Corporation, Armonk, NY, USA). Results are reported as mean ± standard error of mean (SEM).

All variables were checked for outliers, and the normality of their distribution was assessed using the Shapiro-Wilk test and homogeneity of variances using Levene's test. Non-normally distributed variables were transformed using the Tukey Ladder of Powers, as appropriate. Final sample sizes for each parameter are reported in Supplementary

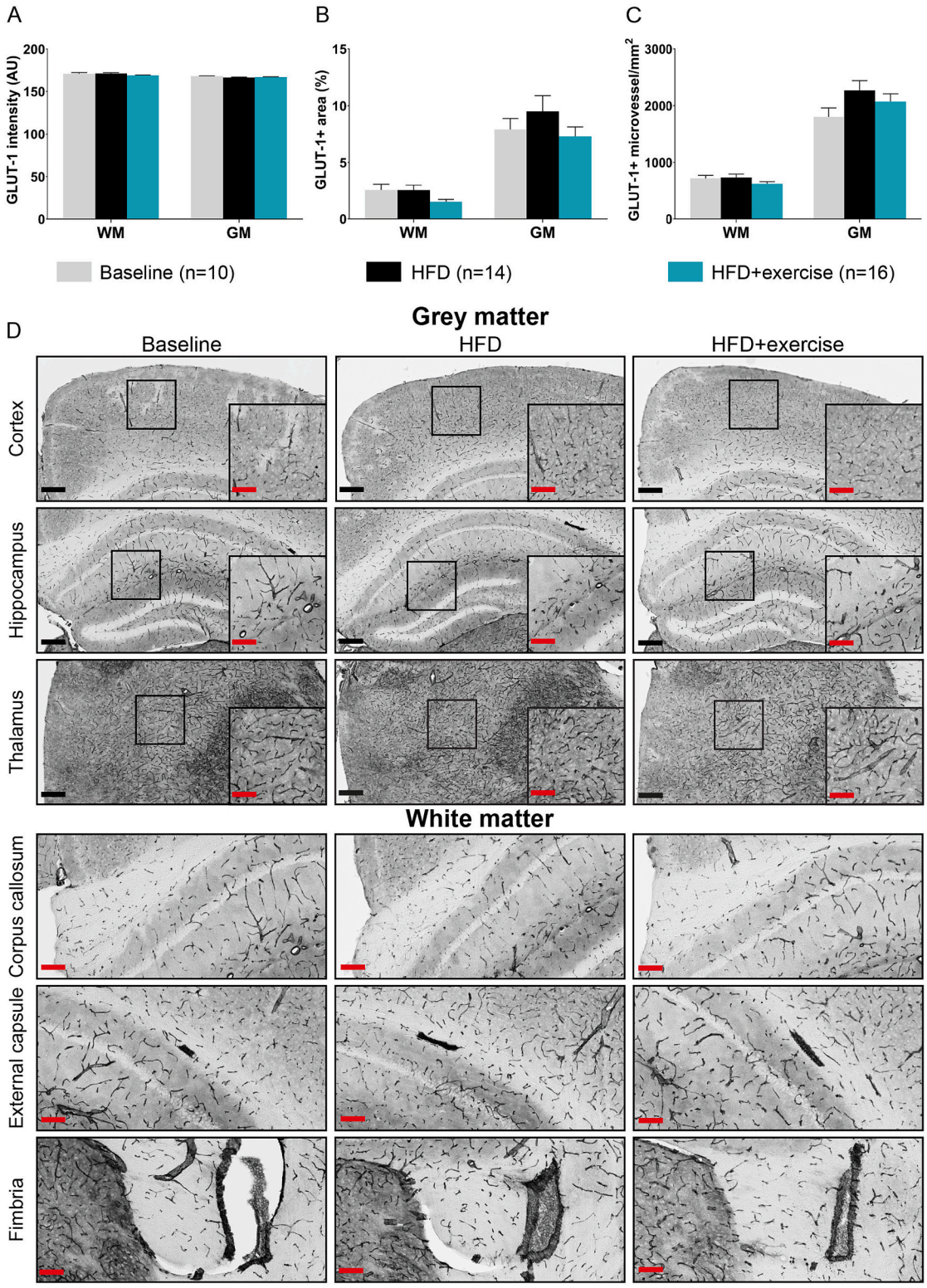

Fig. 2. Microvascular integrity. GLUT-1 immunohistochemistry revealed no significant differences among groups in staining intensity (A), relative area (B), and vessel density (C) in white matter (WM) or grey matter (GM). (D) Representative images: GM at 20× overview with regions of interest (ROI; black squares) and 40× inserts; WM at 40× overview. (Scale bars: red = 100μm; black = 200μm). HFD = high-fat diet; AU = arbitrary units. Values are mean ± SEM.

Table S2, and reasons for exclusion are detailed in Supplementary Table S3.

Multivariate analysis of variance (ANOVA) with Bonferroni correction was applied for multiple group comparisons in WM and GM for normally distributed variables to evaluate group differences. For variables that were not normally distributed, the Independent-Samples Kruskal-Wallis test was used to examine group differences. As WM and GM regions consisted of several subregions, we described group comparisons across sub-regions in Supplementary material including Supplementary Figs. S2-8. Supplementary Table S9 describes sample size per parameter per sub-region.

Before correlation analysis, data were sorted by group and region (WM and GM), and split accordingly to allow separate correlation analysis within each region of each group. Spearman correlation coefficients were used to analyze the correlation among pathology (IHC and PLI) and MRI.

A p-value <0.05 was considered statistically significant for both the ANOVA and Kruskal-Wallis tests, indicating meaningful group differences, and p-value <0.01 for correlation analysis. Further statistical details per outcome are reported in Supplementary Tables S10–S15.

3. Results

3.1. The effect of voluntary exercise on obesity-related pathology and imaging changes

3.1.1. Microvasculature

To investigate **microvascular integrity** in both WM and GM, we performed immunohistochemical staining for GLUT-1 (Fig. 2). No significant differences were observed across groups in GLUT-1 staining intensity, relative area, and GLUT-1+ microvascular density in WM and GM overall (Fig. 2A-C). Similarly, GLUT-1 mRNA expression in GM showed no group differences (results in Supplementary Fig. S1).

Tight junction integrity in endothelial cells was assessed by ZO-1 staining (Fig. 3). ZO-1+ vessel density was higher in GM of HFD mice compared to baseline (Fig. 3D), whereas the HFD+exercise group did not differ significantly from either group. Other ZO-1 staining parameters and mRNA expression showed no group differences (Fig. 3A-C; Supplementary Fig. S1).

3.1.2. Neuroinflammation

We determined **microgliosis** through IBA-1 immunohistochemistry in WM and GM (Fig. 4). In GM, HFD mice showed lower IBA-1 intensity, larger positive area, and smaller cell size compared to baseline (Fig. 4A-C). Both HFD and HFD+exercise groups exhibited higher microglial density than baseline in GM (Fig. 4D) and the HFD group also in WM (Fig. 4D). Cell circularity did not differ among groups (Fig. 4E). No group differences were observed in IBA-1 mRNA expression in GM regions (Supplementary Fig. S1). Although exercise did not normalize microglial density, the absence of significant changes in cell size and area compared to baseline suggests a partial mitigating effect.

We assessed **astrocyte mediated neuroinflammation** via GFAP immunohistochemistry (Fig. 5). Both HFD and HFD+exercise groups showed lower GFAP intensity than the baseline group in WM (Fig. 5A). In contrast, in GM, both HFD and HFD+exercise groups exhibited a larger relative area of GFAP+ staining than the baseline group (Fig. 5B). No group differences were observed in GFAP mRNA expression in GM regions (Supplementary Fig. S1).

3.1.3. Axonal and myelin integrity in white and grey matter

Axonal integrity was evaluated using NfL immunohistochemistry (Fig. 6), as NfL loss reflects axonal damage. HFD mice showed lower NfL intensity in GM compared to baseline group (Fig. 6A). Both HFD and HFD+exercise groups exhibited WM axonal alterations (Fig. 6B). Exercise did not fully prevent axonal changes, but NfL intensity in GM of the exercise group was closer to baseline, indicating partial protection.

We performed PLI to assess **myelin integrity** parameters such as myelin orientation and density in WM and GM (Fig. 7). PLI revealed no significant group differences in myelin dispersion or density (Fig. 7A-B), indicating preserved myelin architecture despite axonal alterations measured with NfL.

3.1.4. MRI

Among the sequences analyzed (T1-weighted, T2-weighted, T2*-weighted, DWI, ADC, and DTI), only T2-weighted imaging showed significant group differences (Fig. 8). T2-weighted signal intensity was reduced in WM of HFD compared to baseline. In HFD+exercise mice, T2-weighted intensity was lower in both WM and GM. No further significant group differences were observed in T1-weighted, T2*-weighted, or diffusion metrics (DTI, DWI, ADC).

3.2. Co-registration between pathology and imaging

To link pathological alterations with imaging findings, we co-registered MRI with IHC and PLI data for correlation analysis. Vascular markers (GLUT-1 and ZO-1) revealed no significant correlations with MRI metrics.

In GM of HFD+exercise mice, microglial density correlated negatively with MD (Rho (ρ) coefficient $= -0.63$; $p<0.01$) and AD (ρ coefficient $= -0.63$; $p<0.01$). No significant correlations were found in WM between neuroinflammatory markers and MRI measures.

In WM of the baseline group, NfL+ area correlated positively with RD (ρ coefficient $= 0.77$; $p<0.01$). No further correlations were observed in GM.

4. Discussion

This study examined whether voluntary exercise mitigates obesity-induced brain alterations in Ldlr-/-.Leiden mice upon HFD feeding. HFD feeding induced pathological features linked to cSVD, such as microvascular changes, glial activation, and axonal injury, although the extent of HFD-induced changes per se cannot be determined within the scope of this study. Because the baseline group is not age-matched with dietary groups, baseline comparisons are used as physiological reference, whereas the exercise effect is evaluated by endpoint-matched HFD vs HFD+exercise comparison. Notably, voluntary exercise exerted region- and cell-type-specific neuroprotective effects: it partially attenuated microgliosis and axonal alterations, particularly in grey matter, suggesting a modulatory role in neuroinflammatory and neurodegenerative processes. Briefly, we observed signs of microgliosis such as larger IBA-1+ cell area in GM under HFD feeding, which was attenuated with exercise. Despite persistent structural imaging abnormalities, exercising mice showed distinct pathology-MRI correlations. In the baseline mice, NfL+ area in WM correlated positively with RD, indicating that RD may capture aspects of axonal architecture rather than myelin integrity alone. In the HFD+exercise mice, higher microglial density in GM correlated with lower MD and AD, which may reflect increased cellularity from neuroinflammation. Whether this represents detrimental gliosis or an adaptive, reparative response to exercise remains to be clarified. To our knowledge, this is the first study to integrate pathology and MRI to explain neuroinflammatory mechanisms underlying GM microstructural changes in an obesity model, and to demonstrate that voluntary exercise may modulate specific pathological and imaging features to a certain extent.

4.1. The effect of voluntary exercise on obesity-related pathology and imaging changes

Prolonged HFD feeding in the Ldlr-/-.Leiden mice induces marked systemic metabolic disturbances, including hyperglycemia, dyslipidemia, and elevated blood pressure, that are not immediately reversed by voluntary exercise (i.e., wheel running). Accordingly, the absence of

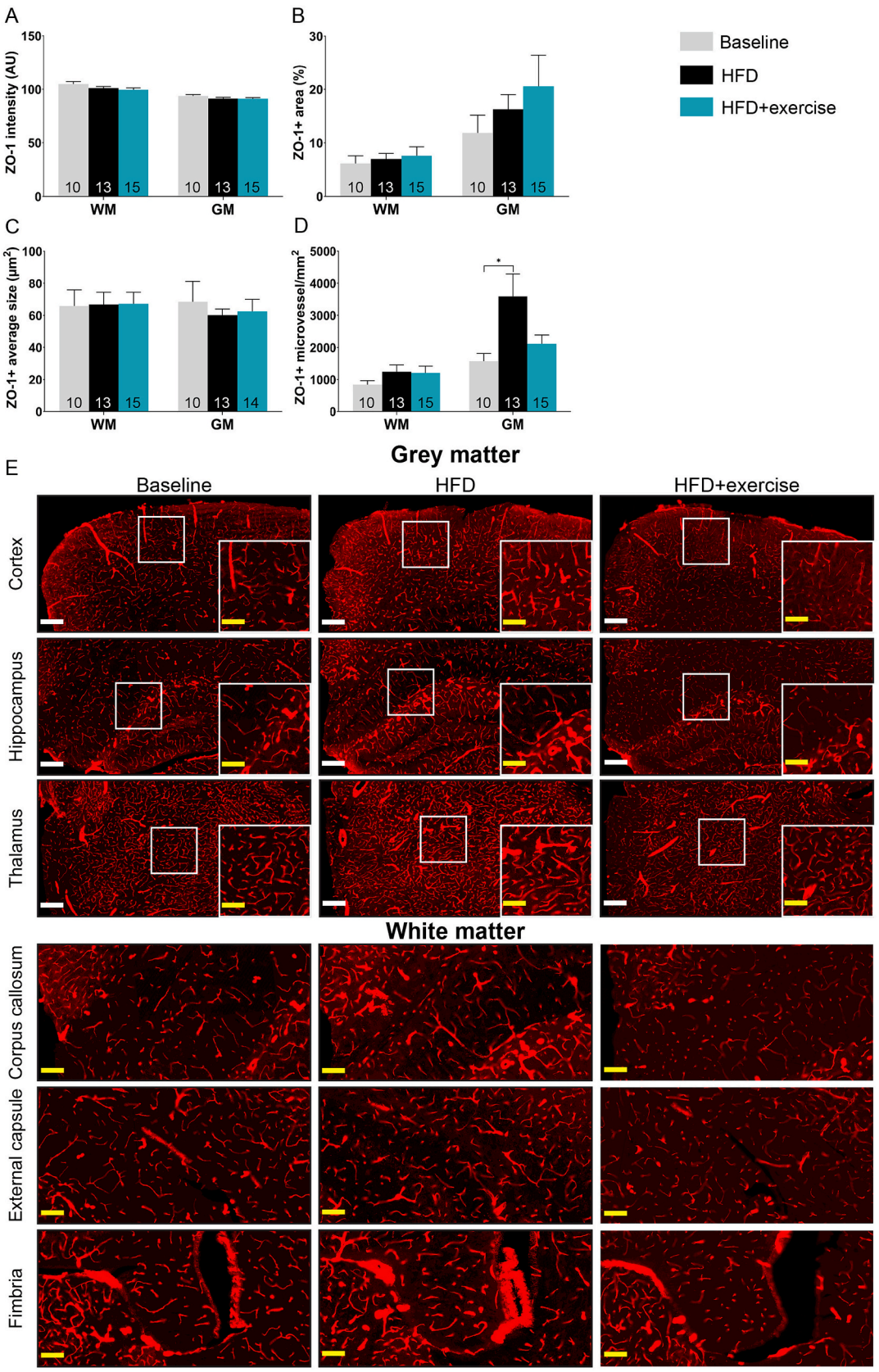

Fig. 3. Tight junction integrity. Zonula occludens-1 (ZO-1) immunohistochemistry showed higher ZO-1+ vessel density in grey matter (GM) in the High-fat diet (HFD) mice versus baseline ($p < 0.05$; D). No significant group differences were found for staining intensity (A), relative area (B), or average size (C). (E) Representative images: GM at 20× overview with regions of interest (ROI; white squares) and 40× inserts; WM at 40× overview. (Scale bars: yellow = 100μm; white = 200μm). AU = arbitrary units. Values are mean ± SEM. *$p < 0.05$.

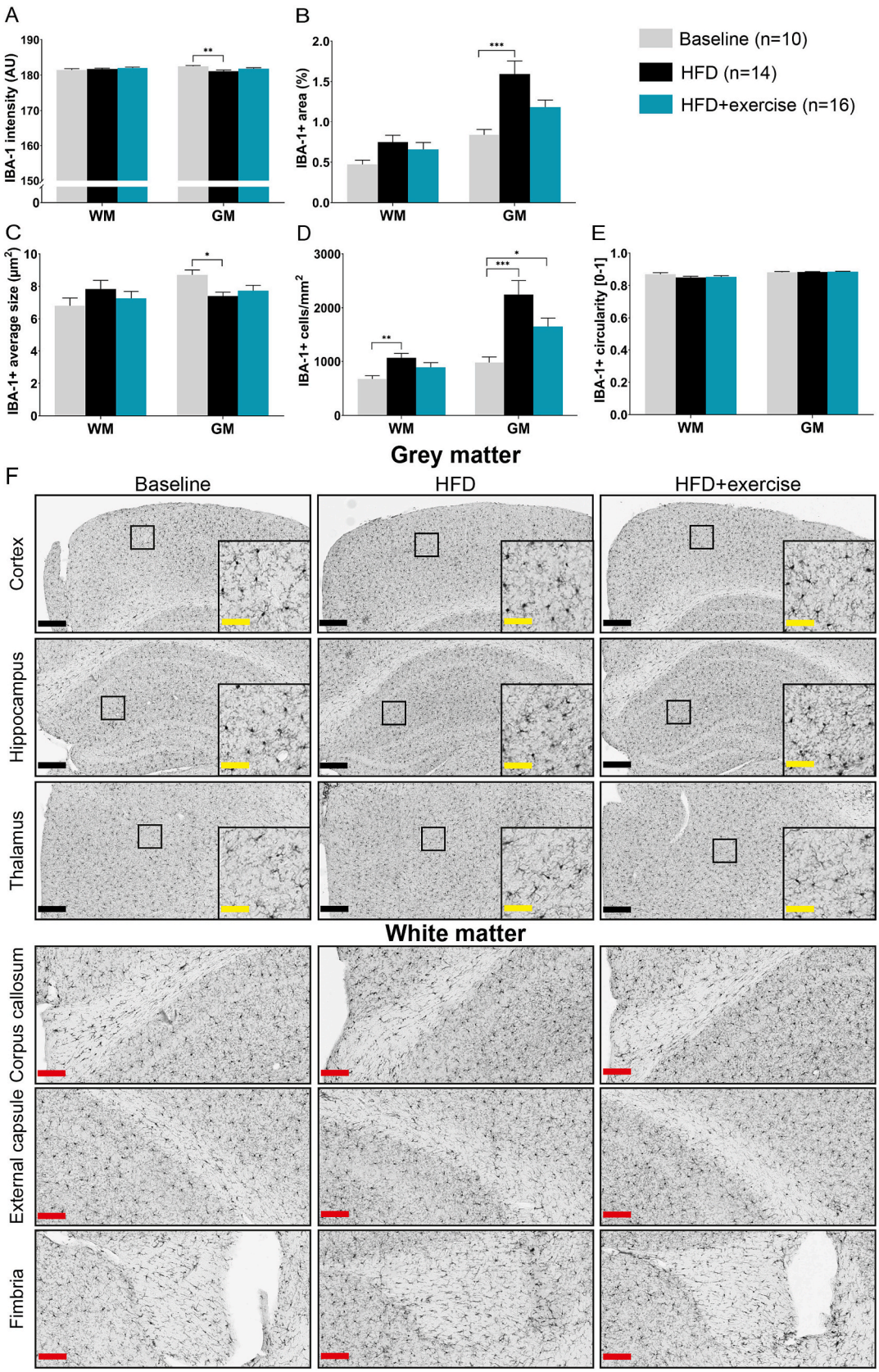

Fig. 4. Neuroinflammation. Ionized calcium-binding adapter molecule-1 (IBA-1) immunohistochemistry showed increased microglial density in grey matter (GM) of both high-fat diet (HFD) and HFD+exercise groups compared to baseline (D), and in white matter (WM) of HFD mice (D). HFD mice also exhibited slightly lower IBA-1 staining intensity (A), larger relative area (B), and smaller average cell size (C) in GM. No group differences were found in cell circularity (E). (F) Representative images: GM at 20× overview with regions of interest (ROIs; black squares) and 80× inserts; WM at 40× overview. (Scale bars: yellow = 50µm; red = 100µm; black = 200µm). AU = arbitrary units. Values are mean ± SEM. *$p < 0.05$, **$p < 0.01$, ***$p < 0.001$.

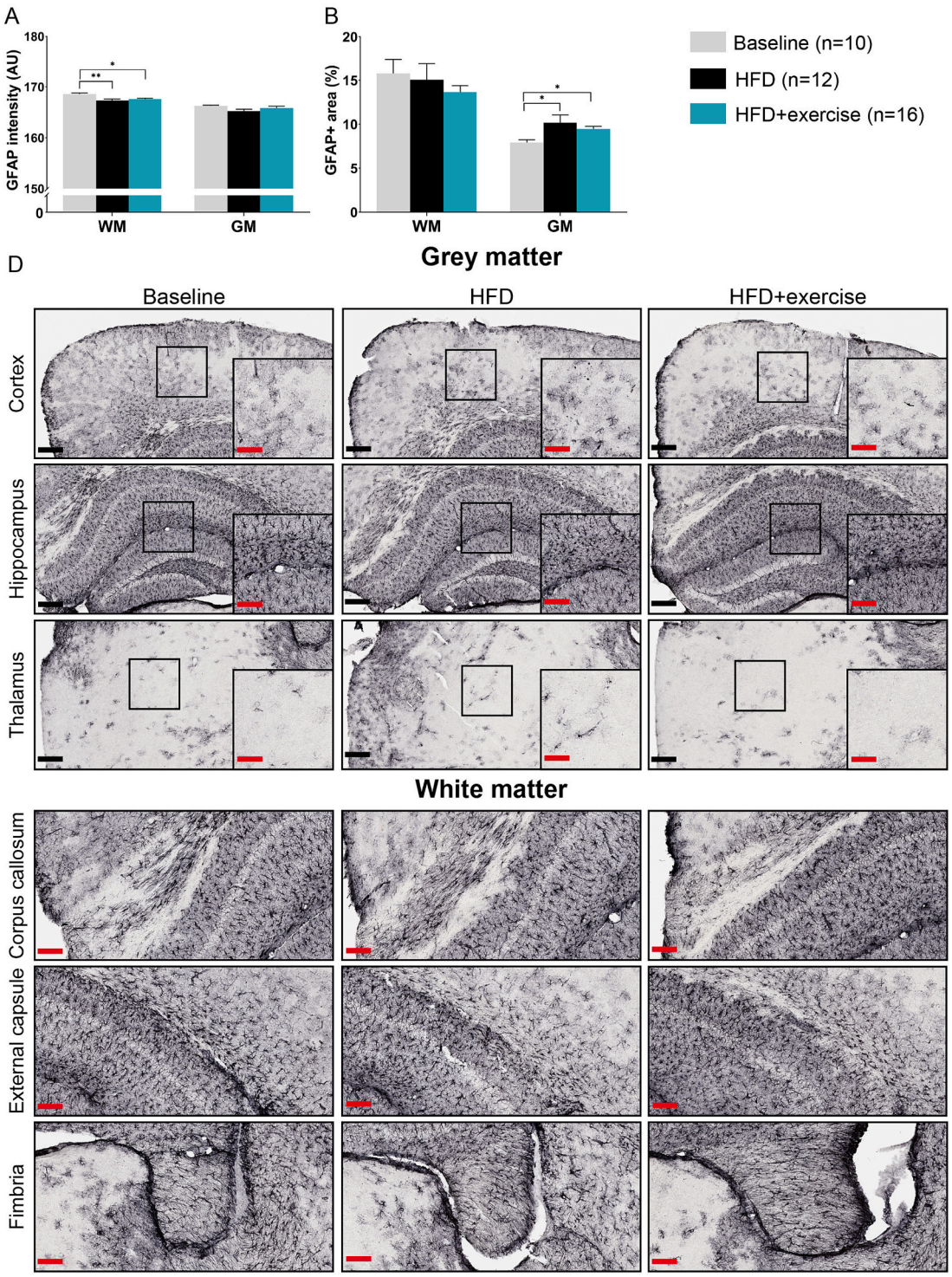

Fig. 5. Neuroinflammation. Glial fibrillary acidic protein (GFAP) immunohistochemistry showed lower staining intensity in white matter (WM) (A) and larger positive area in grey matter (GM) for both high-fat diet (HFD) and HFD+exercise groups compared to baseline (B). (C) Representative images: GM at 20× overview with regions of interest (ROIs; black squares) and 40× inserts; WM at 40× overview. (Scale bars: red = 100μm; black = 200μm). AU = arbitrary units. Values are mean ± SEM. *$p < 0.05$, **$p < 0.01$.

metabolic differences between HFD and HFD+exercise in our study is consistent with the expected systemic phenotype of this model (Morrison et al., 2018; van den Hoek et al., 2020). Importantly, this does not preclude detecting exercise-associated effects in the brain as neurovascular, inflammatory, and microstructural pathways may remain responsive even when systemic metabolic parameters do not normalize, potentially manifesting as modest and region-specific changes.

4.1.1. *Microvasculature*

BBB integrity depends on the structural and functional integrity of microvascular endothelial cells and their intercellular tight junctions (Dodelet-Devillers et al., 2009). In contrast to previous reports (Obadia et al., 2022; Tarantini et al., 2018; Tucsek et al., 2014), we did not detect changes in GLUT-1 protein distribution and mRNA expression across groups, possibly reflecting compensatory mechanisms after prolonged

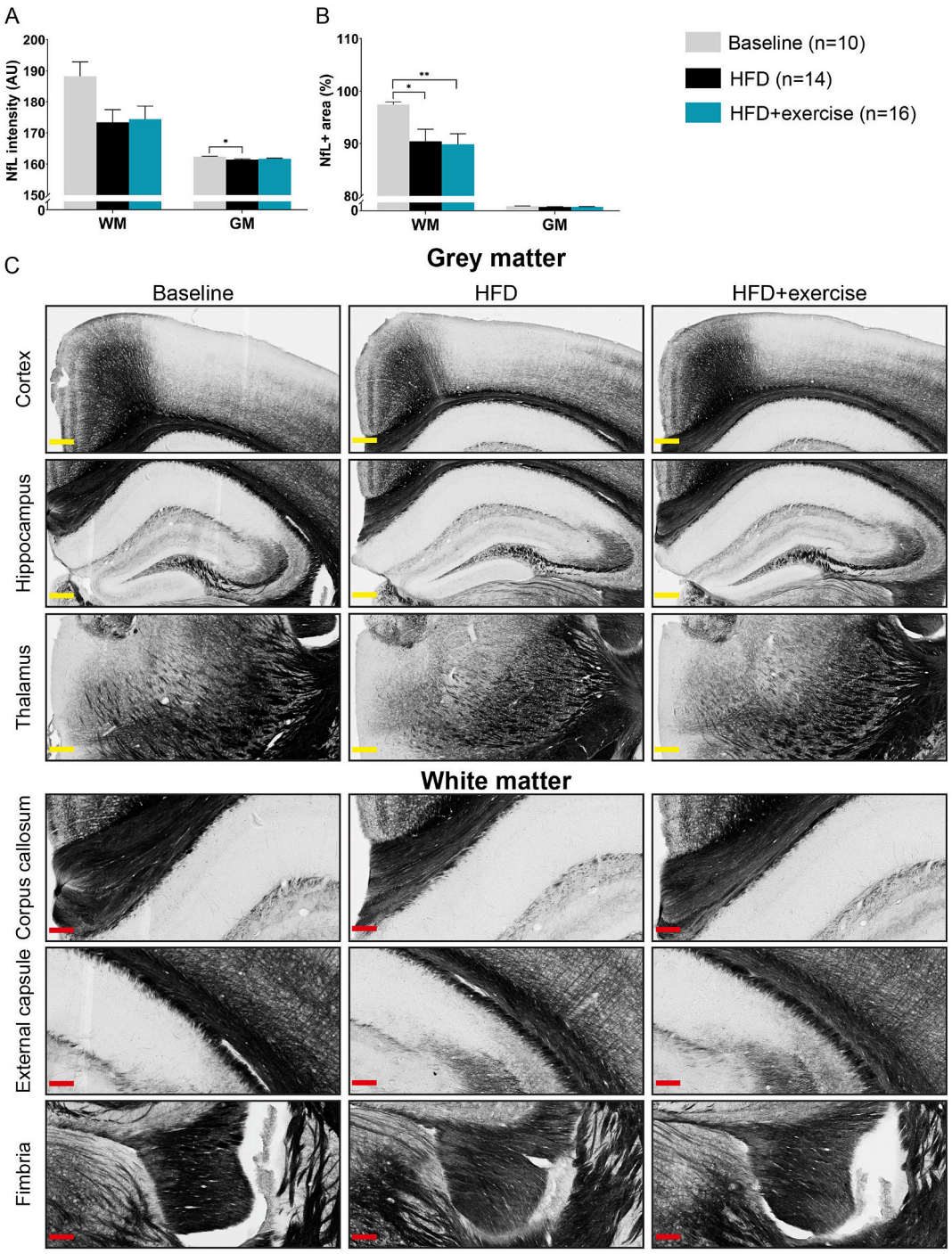

Fig. 6. Axonal integrity. Neurofilament light chain protein (NfL) immunohistochemistry revealed lower staining intensity in grey matter (GM) of high-fat diet (HFD) mice (A) and smaller NfL+ area in white matter (WM) of both HFD and HFD+exercise groups compared to baseline (B). (C) Representative images: GM at 20× overview with regions of interest (ROIs; black squares) and 40× inserts; WM at 40× overview. (Scale bars: red = 100μm; yellow = 200μm). AU = arbitrary units. Values are mean ± SEM. *$p < 0.05$, **$p < 0.01$.

HFD exposure (Jais et al., 2016). HFD+exercise mice showed subregion-specific lower GLUT-1+ intensity in the corpus callosum and lower GLUT-1+ area in the external capsule compared to HFD mice (Supplementary Fig. S2). These findings may reflect adaptative microvascular remodeling; however, it remains unclear whether reduced GLUT-1 is actually linked to more efficient glucose handling. Further work integrating additional microvascular markers will be needed to determine the direction and functional implications of these exercise-associated changes. ZO-1+ microvascular density was increased in GM of HFD mice compared to the baseline group. While this may reflect adaptative microvascular remodeling in response to HFD to preserve oxygen and nutrient supply, age-related vascular changes cannot be excluded, as HFD-fed animals were older than the younger baseline group, which limits direct comparison. An increasing number of studies indicate that chronic high-caloric intake induces cerebrovascular remodeling, including increased vessel density and tortuosity, which may impair blood flow recovery and worsen ischemic vulnerability (Cao et al., 2019; Li et al., 2025; Yi et al., 2012). The apparent regional specificity of this effect may be partly driven by astrocytic modulation, as perivascular astrocytes in GM can promote tight junction protein

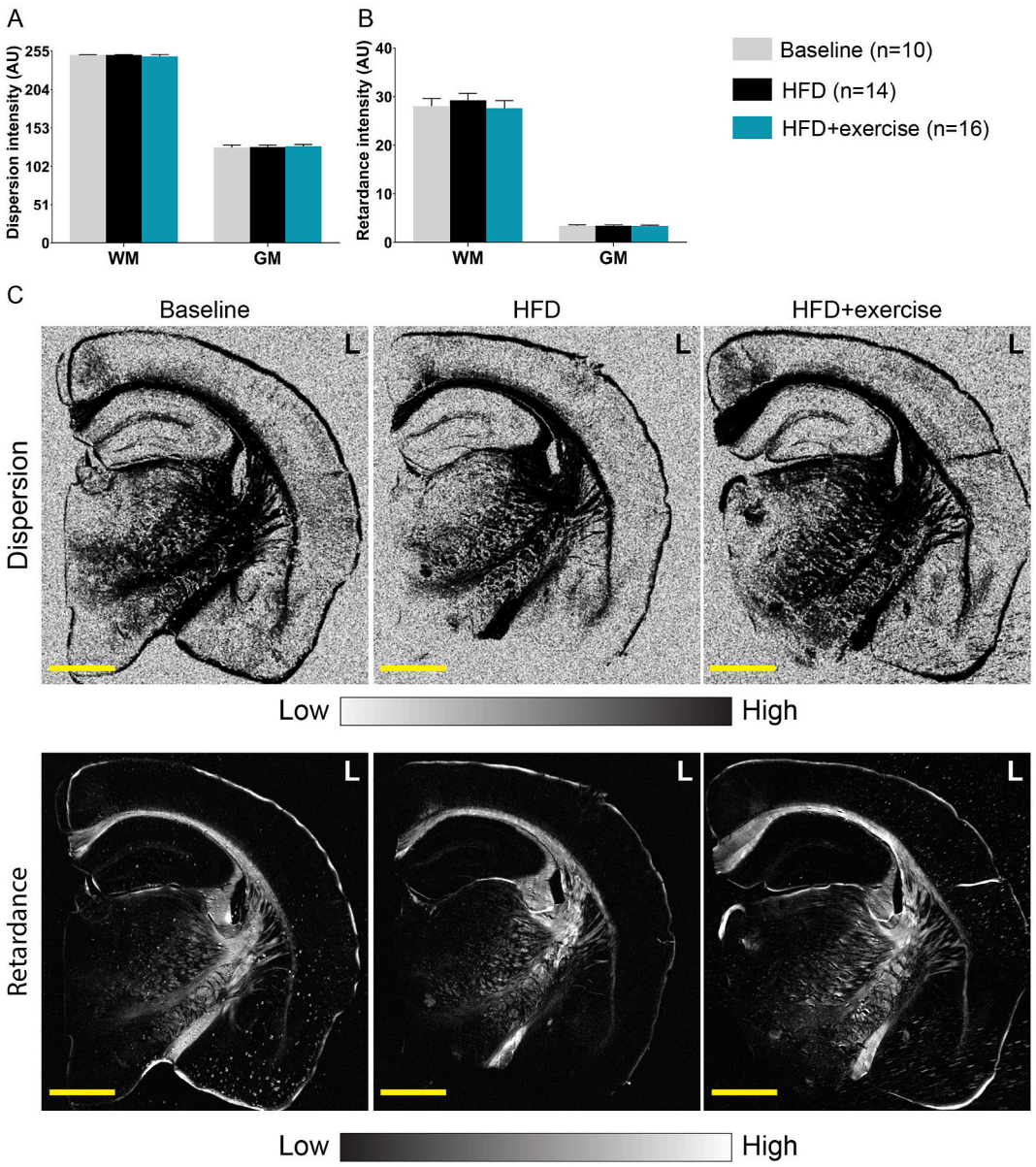

Fig. 7. Myelin orientation and density. Polarized light imaging (PLI) revealed no significant differences in myelin dispersion (A) or density (retardance; B) in white or grey matter (WM resp. GM). (C) Representative images displaying PLI dispersion and retardance. (Yellow scale bars = 1mm). High-fat diet (HFD). Arbitrary units (AU). Values are mean ± SEM.

expression via the release of soluble factors (Abbott et al., 2006; Alvarez et al., 2011; Prat et al., 2001). An increase in ZO-1 density was observed in the HFD group, but not in the HFD+exercise mice. While this may suggest that voluntary exercise attenuates HFD-induced microvascular remodeling and help preserve BBB, this interpretation should be made with caution since no statistically significant difference was detected between HFD and HFD+exercise. Nonetheless, the observed pattern is consistent with a previous report indicating that exercise promotes vascular health and can restore microvascular integrity in ischemic models (Ahn et al., 2016). Together, these results point toward a partial protective effect of exercise, which may require greater intensity or longer duration to achieve statistically robust differences indicating full reversal.

4.1.2. Neuroinflammation

Microglia and astrocytes are key mediators of HFD-induced neuroinflammation (Lama et al., 2022). We observed that six months of HFD feeding increased microgliosis in both WM and GM consistent with previous reports (Jantzen et al., 2024; Kim et al., 2019; Lama et al., 2022; Rong et al., 2025; Wu et al., 2022). We observed higher IBA-1+ cell density in WM and GM and enlarged IBA-1+ cell area in GM in HFD, indicating microgliosis. Interestingly, despite these changes, microglial morphology did not shift toward an amoeboid state, suggesting a more complex activation spectrum (Vidal-Itriago et al., 2022; Waller et al., 2019; Wittekindt et al., 2022). IBA-1 staining intensity was lower in HFD mice, yet mRNA levels remained unchanged, highlighting a possible dissociation between transcript and protein expression (Richardson, 1993). Consistent with previous studies (Zhang et al., 2022), voluntary exercise appeared to attenuate certain microglial alterations as the HFD+exercise group did not differ significantly from the baseline group in IBA-1+ relative area or cell size, in contrast to the HFD group. However, microglial density remained elevated in HFD+exercise mice, suggesting that voluntary exercise mitigated some, but not all, of the observed changes.

On the other hand, signs of astrogliosis (Lama et al., 2022; Paiva et al., 2024) were affected in both HFD and HFD+exercise groups versus

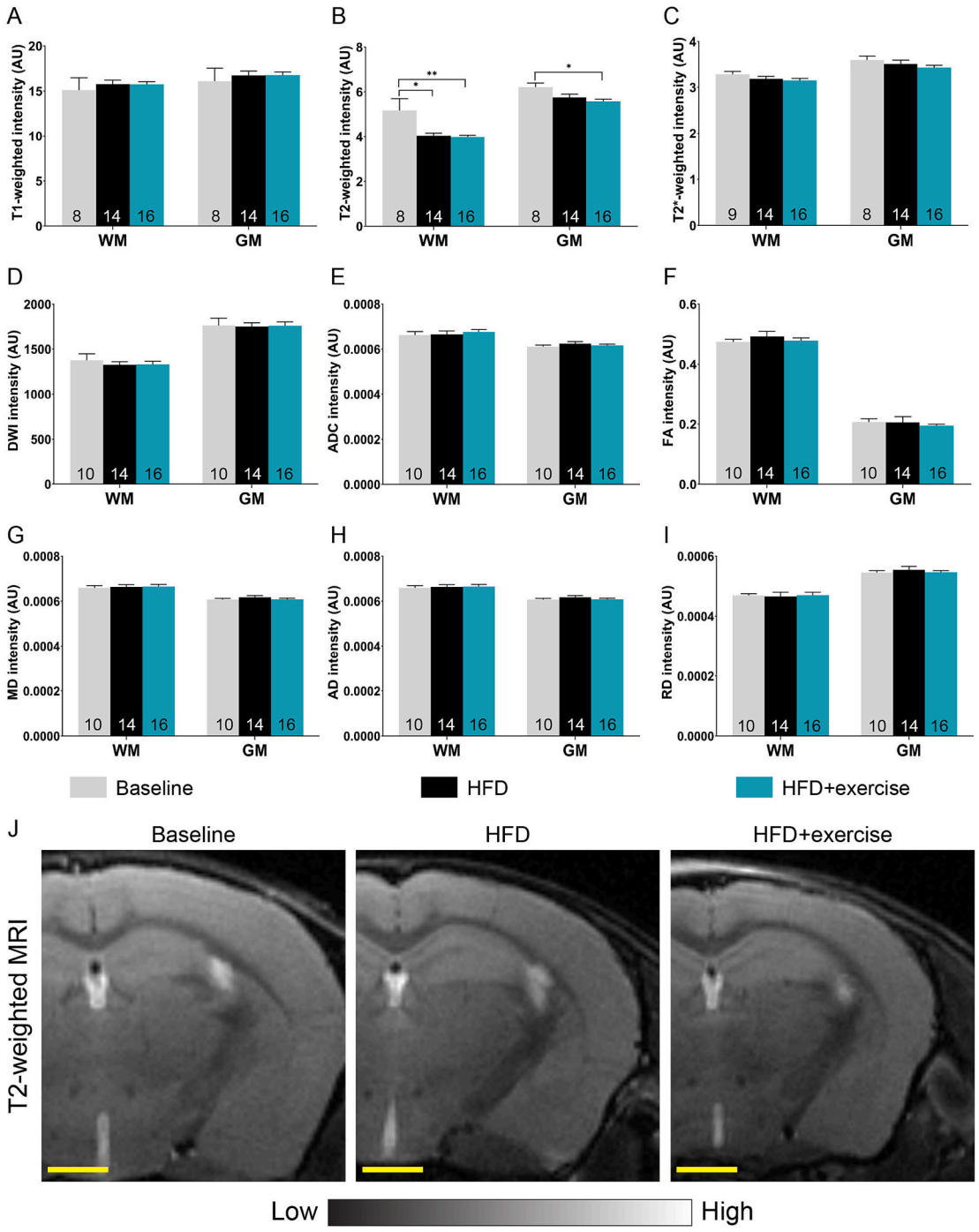

Fig. 8. MRI signal intensity changes. Among the sequences analyzed (A–I), only T2-weighted imaging (B) showed significant group differences: white matter (WM) intensity was lower in the high-fat diet (HFD) mice vs baseline, and both WM and grey matter (GM) intensities were lower in HFD+exercise vs baseline. No significant differences were observed in T1-weighted, T2*-weighted, or diffusion metrics (A, C-I). (J) Representative images displaying T2-weighted MRI. (Yellow scale bars = 1mm). Arbitrary units (AU). Values are mean ± SEM. * $p < 0.05$, ** $p < 0.01$.

baseline. Both groups showed lower GFAP staining intensity in WM and larger GFAP+ area in GM. Despite this regional heterogeneity, voluntary exercise did not appear sufficient to normalize these astrocytic alterations. Notably, we also observed lower T2-weighted intensity in WM of both HFD and HFD+exercise mice, and also in GM of HFD+exercise mice. Previous studies have suggested that increased glial cell density and reduced extracellular space can shorten T2 relaxation times, and consequently lower signal intensity (Hoch et al., 2016; Miwa et al., 2003; Roitbak and Sykova, 1999). In this context, these effects may reflect gliosis-related microstructural changes. Although the exact mechanism remains unclear, our results suggest that gliosis may be one of the contributing factors to MRI signal alterations.

4.1.3. *Axonal and myelin integrity*

Using NfL staining, we observed aging and HFD-induced axonal damage in both WM and GM. NfL is a structural axonal protein that is released into the bloodstream and cerebrospinal fluid (CSF) following axonal damage (Kahn et al., 2025). Accordingly, increased NfL levels are widely reported in the blood and CSF of individuals with Alzheimer's disease and mouse models (Kotredes et al., 2024; Mielke et al., 2025;

Olsson et al., 2016). However, little is known about NfL distribution within brain tissue during early pathology. In our study, we observed that HFD led to lower NfL staining intensity in GM and smaller relative area of NfL+ in WM compared to baseline. These findings indicate early axonal disruption in both WM and GM of HFD-fed mice. While no significant differences were observed between HFD and HFD+exercise mice, NfL intensity in GM of the HFD+exercise group was similar to the baseline group, suggesting partial restoration by voluntary exercise. Longer exercise intervention periods or combined lifestyle strategies (e.g., diet) could be considered in future studies to assess voluntary exercise potential in mitigating HFD-induced axonal damage.

PLI measures, reflecting myelin integrity (Mollink et al., 2019), showed no significant group differences, suggesting gross myelin architecture was preserved. Similarly, DTI metrics commonly used to assess axonal and myelin integrity also demonstrated no group differences. Although clinical studies link NfL and DTI in symptomatic neurodegenerative patients (Qin et al., 2024; Schultz et al., 2020), these associations may not apply to early-stage changes. Together with imaging data, these findings suggest that axonal pathology precedes MRI-detectable alterations, supporting NfL as an early marker of axonal injury.

4.2. Co-registration between pathology and imaging

In baseline mice, we observed a positive correlation between NfL+ area and RD in WM. Although RD is often associated with myelin damage (Song et al., 2005), evidence from multiple sclerosis studies and our findings suggest RD also reflects axonal integrity (Klawiter et al., 2011). Higher NfL+ area was associated with increased RD, further proposing that RD is not specific for assessing myelin integrity, but is also sensitive for assessing axonal integrity. However, more research is needed in the future to further interpret RD.

In HFD+exercise mice, we found that IBA-1+ microglial density in GM was negatively correlated with diffusion metrics, including MD and AD. MD reflects the average diffusion rate of water molecules (Bennett and Madden, 2014), and although it is primarily used for WM integrity, it can also indicate GM microstructural changes (Henf et al., 2018). Clinical studies showed that MD changes in cortex can reflect neuroinflammation such as astrogliosis (Vilaplana et al., 2020), as increased glial density alters extracellular diffusion properties (Montal et al., 2018). However, to our knowledge, this negative correlation between microglial density and MD in GM has not been previously confirmed in such model. In the HFD+exercise group, we also found negative correlation between microglial density and AD in GM. Although AD is considered for axonal integrity (Kaushal et al., 2019), its interpretation in GM is challenging due to isotropic diffusion (Park et al., 2014), and few studies have explored its link to neuroinflammation. A clinical trial suggested that neuroinflammation may precede axonal degeneration in the GM of Parkinson's disease patients (Andica et al., 2019). Our finding that microglial density in GM of HFD+exercise mice negatively correlated with both MD and AD provides novel evidence linking neuroinflammation to GM microstructural changes. In addition, FA (metric for microstructural integrity (Bennett and Madden, 2014)) showed subregional group differences (Supplementary Fig. S8). We observed lower FA in the fimbria of HFD+exercise mice compared to HFD, while values did not differ from the baseline group. Although comparison to baseline should be interpreted with caution, this pattern suggests that exercise may partially shift white matter microstructural integrity away from HFD-associated effects. Future studies incorporating tractography-matched histology will be required to determine which microstructural features drive this FA change.

4.3. Limitations

This study has several limitations. The primary limitation is the absence of an age-matched non-obese control group, limiting the ability to fully separate obesity- from age-related changes. Therefore, the results should be interpreted with caution. Although the baseline group is not age-matched to the experimental groups, it was meant to serve as a physiological reference prior to interventions, representing a young non-obese adult brain. As such, it offers insight into the direction and extent of pathological changes induced by prolonged HFD exposure. Importantly, animals in the experimental groups (HFD-fed) were the same age at the time of analyses, allowing for consistent age comparisons across HFD and HFD+exercise conditions. In addition, our main aim was to assess the impact of HFD and exercise, rather than aging per se, which was comprehensively assessed in a previous study (Seidel et al., 2025). Consistent with this earlier research which demonstrated a stronger impact of HFD than aging alone (Seidel et al., 2025), HFD feeding in the present study led to obesity, increased systolic blood pressure, hyperglycemia and hypercholesterolemia (Supplementary Table S4). Nevertheless, future research including age-matched non-obese controls is warranted to strengthen the broad applicability and better disentangle obesity- and age-related effects. Second, voluntary exercise resulted in modest neuroprotective effects. We observed several consequences of aging and prolonged HFD exposure in HFD mice versus baseline, yet some of these did not occur under voluntary exercise. Based on these observations, we inferred that those in the voluntary exercise group remained similar to the younger non-obese baseline mice, and thereby voluntary exercise led to beneficial effects. However, we acknowledge that differences did not reach significant among HFD groups, implying that voluntary exercise was not sufficient to reverse the observed effects. Future studies could explore whether longer intervention periods or combined lifestyle strategies (e.g., diet) lead to additional improvements. Future studies could also explore the effects of specific training protocols (e.g. regular bouts of vigorous exercise versus endurance training). In the present study, mice exercised voluntarily which does not allow direct translation to specific forms of training in humans.

5. Conclusion

Ldlr-/-.Leiden mice consuming HFD long-term demonstrated cSVD-related changes, including region-specific microvascular remodeling, glial activation, and axonal injury. Voluntary exercise exerted partially neuroprotective effects by attenuating microgliosis, and preserving axonal integrity and subregion-specific effects associated with microvascular and microstructural changes predominantly in white matter. Importantly, the present work integrates pathology and MRI through precise spatial co-registration, providing a multimodal framework that directly links microscopic alteration to imaging metrics. This approach offers mechanistic insight into how diffusion and T2-weighted signals reflect early obesity-related neurovascular changes. Collectively, these findings refine interpretation of commonly used MRI markers and demonstrate that even modest, voluntary exercise induces spatially selective neurovascular and microstructural adaptations. While future research is warranted with more intense or longer exercise, these findings underscore the value of multimodal approaches to unravel obesity-related brain pathology and guide the development of targeted interventions.

Institutional Review Board Statement: This animal study was approved by the Central Authority for Scientific Procedures on Animals (CCD, The Hague, the Netherlands; approval number: AVD5010020172064). Ethical approval was provided by the TNO Animal Welfare Body (TNO, the Netherlands; Permit number: TNO-476) and the Veterinary Authority of the Radboud university medical center (Nijmegen, the Netherlands; approval number: 2020-0033-001).

Informed Consent Statement: Not applicable.

Funding

This research was funded by a ZonMw grant (Program: Enabling Technologies Hotels; number: 435005011) and the TNO research program 'PMC Brain Health').

CRediT authorship contribution statement

Xiaoxue Liang: Writing – review & editing, Writing – original draft, Visualization, Methodology, Investigation, Formal analysis, Conceptualization. **Klara J. Lohkamp:** Writing – review & editing, Methodology, Investigation. **Anita M. van den Hoek:** Writing – review & editing, Conceptualization. **Bram Geenen:** Writing – review & editing, Methodology, Investigation. **Vivienne Verweij:** Writing – review & editing, Methodology, Investigation. **Martine C. Morrison:** Writing – review & editing, Conceptualization. **Robert Kleemann:** Writing – review & editing, Supervision, Project administration, Funding acquisition, Conceptualization. **Amanda J. Kiliaan:** Writing – review & editing, Writing – original draft, Supervision, Project administration, Methodology, Investigation, Funding acquisition, Conceptualization. **Maximilian Wiesmann:** Writing – review & editing, Writing – original draft, Supervision, Investigation, Funding acquisition, Conceptualization. **Gemma Solé-Guardia:** Writing – review & editing, Writing – original draft, Visualization, Supervision, Methodology, Investigation, Formal analysis, Data curation, Conceptualization.

Declaration of Competing Interest

The authors declare that they have no known competing financial interests or personal relationships that could have appeared to influence the work reported in this paper.

Acknowledgements

We gratefully acknowledge Tecnilab-BMI for providing the running wheels for this study. The authors thank the biotechnicians at the Animal Research Facility of the Radboud University Medical Center for taking excellent care of the mice.

Appendix A. Supplementary data

Supplementary data to this article can be found online at https://doi.org/10.1016/j.bbi.2026.106539.

Data availability

Data will be made available on request.

References

Abbott, N.J., Ronnback, L., Hansson, E., 2006. Astrocyte-endothelial interactions at the blood-brain barrier. Nat. Rev. Neurosci. 7, 41–53.

Abu-Rumeileh, S., Abdelhak, A., Foschi, M., D'Anna, L., Russo, M., Steinacker, P., Kuhle, J., Tumani, H., Blennow, K., Otto, M., 2023. The multifaceted role of neurofilament light chain protein in non-primary neurological diseases. Brain 146, 421–437.

Afshin, A., Forouzanfar, M.H., Reitsma, M.B., Sur, P., Estep, K., Lee, A., Marczak, L., Mokdad, A.H., Moradi-Lakeh, M., Naghavi, M., Salama, J.S., Vos, T., Abate, K.H., Abbafati, C., Ahmed, M.B., Al-Aly, Z., Alkerwi, A., Al-Raddadi, R., Amare, A.T., Amberbir, A., Amegah, A.K., Amini, E., Amrock, S.M., Anjana, R.M., Ärnlöv, J., Asayesh, H., Banerjee, A., Barac, A., Baye, E., Bennett, D.A., Beyene, A.S., Biadgilign, S., Biryukov, S., Bjertness, E., Boneya, D.J., Campos-Nonato, I., Carrero, J.J., Cecilio, P., Cercy, K., Ciobanu, L.G., Cornaby, L., Damtew, S.A., Dandona, L., Dandona, R., Dharmaratne, S.D., Duncan, B.B., Eshrati, B., Esteghamati, A., Feigin, V.L., Fernandes, J.C., Fürst, T., Gebrehiwot, T.T., Gold, A., Gona, P.N., Goto, A., Habtewold, T.D., Hadush, K.T., Hafezi-Nejad, N., Hay, S.I., Horino, M., Islami, F., Kamal, R., Kasaeian, A., Katikireddi, S.V., Kengne, A.P., Kesavachandran, C.N., Khader, Y.S., Khang, Y.H., Khubchandani, J., Kim, D., Kim, Y. J., Kinfu, Y., Kosen, S., Ku, T., Defo, B.K., Kumar, G.A., Larson, H.J., Leinsalu, M., Liang, X., Lim, S.S., Liu, P., Lopez, A.D., Lozano, R., Majeed, A., Malekzadeh, R., Malta, D.C., Mazidi, M., McAlinden, C., McGarvey, S.T., Mengistu, D.T., Mensah, G. A., Mensink, G.B.M., Mezgebe, H.B., Mirrakhimov, E.M., Mueller, U.O., Noubiap, J. J., Obermeyer, C.M., Ogbo, F.A., Owolabi, M.O., Patton, G.C., Pourmalek, F., Qorbani, M., Rafay, A., Rai, R.K., Ranabhat, C.L., Reinig, N., Safiri, S., Salomon, J.A., Sanabria, J.R., Santos, I.S., Sartorius, B., Sawhney, M., Schmidhuber, J., Schutte, A. E., Schmidt, M.I., Sepanlou, S.G., Shamsizadeh, M., Sheikhbahaei, S., Shin, M.J., Shiri, R., Shiue, I., Roba, H.S., Silva, D.A.S., Silverberg, J.I., Singh, J.A., Stranges, S., Swaminathan, S., Tabarés-Seisdedos, R., Tadese, F., Tedla, B.A., Tegegne, B.S., Terkawi, A.S., Thakur, J.S., Tonelli, M., Topor-Madry, R., Tyrovolas, S., Ukwaja, K. N., Uthman, O.A., Vaezghasemi, M., Vasankari, T., Vlassov, V.V., Vollset, S.E., Weiderpass, E., Werdecker, A., Wesana, J., Westerman, R., Yano, Y., Yonemoto, N., Yonga, G., Zaidi, Z., Zenebe, Z.M., Zipkin, B., Murray, C.J.L., 2017. Health effects of overweight and obesity in 195 countries over 25 years. N. Engl. J. Med. 377, 13–27.

Ahn, J.H., Choi, J.H., Park, J.H., Kim, I.H., Cho, J.H., Lee, J.C., Koo, H.M., Hwangbo, G., Yoo, K.Y., Lee, C.H., Hwang, I.K., Cho, J.H., Choi, S.Y., Kwon, Y.G., Kim, Y.M., Kang, I.J., Won, M.H., 2016. Long-term exercise improves memory deficits via restoration of myelin and microvessel damage, and enhancement of neurogenesis in the aged gerbil hippocampus after ischemic stroke. Neurorehabil. Neural Repair 30, 894–905.

Alvarez, J.I., Dodelet-Devillers, A., Kebir, H., Ifergan, I., Fabre, P.J., Terouz, S., Sabbagh, M., Wosik, K., Bourbonniere, L., Bernard, M., van Horssen, J., de Vries, H. E., Charron, F., Prat, A., 2011. The Hedgehog pathway promotes blood-brain barrier integrity and CNS immune quiescence. Science 334, 1727–1731.

Anderson, M.E., Wind, E.J., Robison, L.S., 2024. Exploring the neuroprotective role of physical activity in cerebral small vessel disease. Brain Res. 1833, 148884.

Andica, C., Kamagata, K., Hatano, T., Saito, A., Uchida, W., Ogawa, T., Takeshige-Amano, H., Zalesky, A., Wada, A., Suzuki, M., Hagiwara, A., Irie, R., Hori, M., Kumamaru, K.K., Oyama, G., Shimo, Y., Umemura, A., Pantelis, C., Hattori, N., Aoki, S., 2019. Free-water imaging in white and gray matter in parkinson's disease. Cells 8.

Arnoldussen, I.A.C., Morrison, M.C., Wiesmann, M., van Diepen, J.A., Worms, N., Voskuilen, M., Verweij, V., Geenen, B., Gualdo, N.P., van der Logt;, L., Gross, G., Kleemann, R., Kiliaan, A.J., 2022. Milk fat globule membrane attenuates high fat diet-induced neuropathological changes in obese Ldlr-/-.Leiden mice. Int. J. Obes. (Lond) 46, 342–349.

Arnoldussen, I.A.C., Wiesmann, M., Pelgrim, C.E., Wielemaker, E.M., van Duyvenvoorde, W., Amaral-Santos, P.L., Verschuren, L., Keijser, B.J.F., Heerschap, A., Kleemann, R., Wielinga, P.Y., Kiliaan, A.J., 2017. Butyrate restores HFD-induced adaptations in brain function and metabolism in mid-adult obese mice. Int. J. Obes. (Lond) 41, 935–944.

Azzolini, F., Gilio, L., Pavone, L., Iezzi, E., Dolcetti, E., Bruno, A., Buttari, F., Musella, A., Mandolesi, G., Guadalupi, L., Furlan, R., Finardi, A., Micillo, T., Carbone, F., Matarese, G., Centonze, D., Stampanoni Bassi, M., 2022. Neuroinflammation Is Associated with GFAP and sTREM2 Levels in Multiple Sclerosis. Biomolecules 12.

Bailey, E.L., Wardlaw, J.M., Graham, D., Dominiczak, A.F., Sudlow, C.L., Smith, C., 2011. Cerebral small vessel endothelial structural changes predate hypertension in stroke-prone spontaneously hypertensive rats: a blinded, controlled immunohistochemical study of 5- to 21-week-old rats. Neuropathol. Appl. Neurobiol. 37, 711–726.

Behler, A., Muller, H.P., Ludolph, A.C., Kassubek, J., 2023. Diffusion tensor imaging in amyotrophic lateral sclerosis: machine learning for biomarker development. Int. J. Mol. Sci. 24.

Bennett, I.J., Madden, D.J., 2014. Disconnected aging: cerebral white matter integrity and age-related differences in cognition. Neuroscience 276, 187–205.

Blair, S.N., Church, T.S., 2004. The fitness, obesity, and health equation: is physical activity the common denominator? J. Am. Med. Assoc. 292, 1232–1234.

Brossard, C., Montigon, O., Boux, F., Delphin, A., Christen, T., Barbier, E.L., Lemasson, B., 2020. MP3: medical software for processing multi-parametric images pipelines. Front. Neuroinf. 14, 594799.

Cao, R., Li, J., Zhang, C., Zuo, Z., Hu, S., 2019. Photoacoustic microscopy of obesity-induced cerebrovascular alterations. Neuroimage 188, 369–379.

Colcombe, S.J., Erickson, K.I., Raz, N., Webb, A.G., Cohen, N.J., McAuley, E., Kramer, A. F., 2003. Aerobic fitness reduces brain tissue loss in aging humans. J. Gerontol. A Biol. Sci. Med. Sci. 58, 176–180.

Defrancesco, M., Egger, K., Marksteiner, J., Esterhammer, R., Hinterhuber, H., Deisenhammer, E.A., Schocke, M., 2014. Changes in white matter integrity before conversion from mild cognitive impairment to Alzheimer's disease. PLoS One 9, e106062.

Dodelet-Devillers, A., Cayrol, R., van Horssen, J., Haqqani, A.S., de Vries, H.E., Engelhardt, B., Greenwood, J., Prat, A., 2009. Functions of lipid raft membrane microdomains at the blood-brain barrier. J. Mol. Med. (Berl) 87, 765–774.

Duering, M., Biessels, G.J., Brodtmann, A., Chen, C., Cordonnier, C., de Leeuw, F.-E., Debette, S., Frayne, R., Jouvent, E., Rost, N.S., ter Telgte, A., Al-Shahi Salman, R., Backes, W.H., Bae, H.-J., Brown, R., Chabriat, H., De Luca, A., deCarli, C., Dewenter, A., Doubal, F.N., Ewers, M., Field, T.S., Ganesh, A., Greenberg, S., Helmer, K.G., Hilal, S., Jochems, A.C.C., Jokinen, H., Kuijf, H., Lam, B.Y.K., Lebenberg, J., MacIntosh, B.J., Maillard, P., Mok, V.C.T., Pantoni, L., Rudilosso, S., Satizabal, C.L., Schirmer, M.D., Schmidt, R., Smith, C., Staals, J., Thrippleton, M.J., van Veluw, S.J., Vemuri, P., Wang, Y., Werring, D., Zedde, M., Akinyemi, R.O., Del Brutto, O.H., Markus, H.S., Zhu, Y.-C., Smith, E.E., Dichgans, M., Wardlaw, J.M., 2023. Neuroimaging standards for research into small vessel disease—advances since 2013. The Lancet Neurology 22, 602–618.

Elsaafien, K., Sloan, J.M., Evans, R.G., Cochrane, A.D., Marino, B., McCall, P.R., Hood, S. G., Yao, S.T., Korim, W.S., Bailey, S.R., Jufar, A.H., Peiris, R.M., Bellomo, R., Miles, L.F., May, C.N., Lankadeva, Y.R., 2023. Associations between systemic and cerebral inflammation in an ovine model of cardiopulmonary bypass. Anesth. Analg. 136, 802–813.

Elzinga, S.E., Guo, K., Turfah, A., Henn, R.E., Webber-Davis, I.F., Hayes, J.M., Pacut, C. M., Teener, S.J., Carter, A.D., Rigan, D.M., Allouch, A.M., Jang, D.G., Parent, R., Glass, E., Murphy, G.G., Lentz, S.I., Chen, K.S., Zhao, L., Hur, J., Feldman, E.L., 2025. Metabolic stress and age drive inflammation and cognitive decline in mice and humans. Alzheimers Dement. 21, e70060.

Evans, L.E., Taylor, J.L., Smith, C.J., Pritchard, H.A.T., Greenstein, A.S., Allan, S.M., 2021. Cardiovascular comorbidities, inflammation, and cerebral small vessel disease. Cardiovasc. Res. 117, 2575–2588.

Feng, Z., Fang, C., Ma, Y., Chang, J., 2024. Obesity-induced blood-brain barrier dysfunction: phenotypes and mechanisms. J. Neuroinflammation 21, 110.
Franklin, K.B., Paxinos, G., 2019. Paxinos and franklin's the mouse brain in stereotaxic coordinates. Compact: The Coronal Plates and Diagrams. Academic Press, Cambridge, MA, USA.
Henf, J., Grothe, M.J., Brueggen, K., Teipel, S., Dyrba, M., 2018. Mean diffusivity in cortical gray matter in Alzheimer's disease: The importance of partial volume correction. Neuroimage Clin 17, 579–586.
Hoch, M., Win, W., Hagiwara, M., Fatterpekar, G., Patel, S., 2016. Orbital lesions with low signal intensity on T2-weighted imaging. Clin. Radiol. 71, e88–e95.
Iannello, F., 2019. Non-intrusive high throughput automated data collection from the home cage. Heliyon 5, e01454.
Jais, A., Solas, M., Backes, H., Chaurasia, B., Kleinridders, A., Theurich, S., Mauer, J., Steculorum, S.M., Hampel, B., Goldau, J., Alber, J., Forster, C.Y., Eming, S.A., Schwaninger, M., Ferrara, N., Karsenty, G., Bruning, J.C., 2016. Myeloid-cell-derived VEGF maintains brain glucose uptake and limits cognitive impairment in obesity. Cell 165, 882–895.
Janssen, C.I., Jansen, D., Mutsaers, M.P., Dederen, P.J., Geenen, B., Mulder, M.T., Kiliaan, A.J., 2016. The effect of a high-fat diet on brain plasticity, inflammation and cognition in female ApoE4-knockin and ApoE-knockout mice. PLoS One 11, e0155307.
Jantzen, L., Dumontoy, S., Ramadan, B., Houdayer, C., Haffen, E., Hichami, A., Khan, N. A., Van Waes, V., Cabeza, L., 2024. Dietary linoleic acid supplementation protects against obesity-induced microglial reactivity in mice. Sci. Rep. 14, 6644.
Jia, R., Solé-Guardia, G., Verweij, V., Snabel, J.M., Geenen, B., Tuladhar, A.M., Kleemann, R., Kiliaan, A.J., Wiesmann, M., 2025. Identification and characterization of a translational mouse model for blood–brain barrier leakage in cerebral small vessel disease. Int. J. Mol. Sci. 26, 6706.
Kahn, O.I., Dominguez, S.L., Glock, C., Hayne, M., Vito, S., Sengupta Ghosh, A., Adrian, M., Burgess, B.L., Meilandt, W.J., Friedman, B.A., Hoogenraad, C.C., 2025. Secreted neurofilament light chain after neuronal damage induces myeloid cell activation and neuroinflammation. Cell Rep. 44, 115382.
Kaushal, M., Shabani, S., Budde, M., Kurpad, S., 2019. Diffusion tensor imaging in acute spinal cord injury: a review of animal and human studies. J. Neurotrauma 36, 2279–2286.
Kim, J.D., Yoon, N.A., Jin, S., Diano, S., 2019. Microglial UCP2 mediates inflammation and obesity induced by high-fat feeding. Cell Metab. 30 (952–962), e955.
Klawiter, E.C., Schmidt, R.E., Trinkaus, K., Liang, H.F., Budde, M.D., Naismith, R.T., Song, S.K., Cross, A.H., Benzinger, T.L., 2011. Radial diffusivity predicts demyelination in ex vivo multiple sclerosis spinal cords. Neuroimage 55, 1454–1460.
Kotredes, K.P., Pandey, R.S., Persohn, S., Elderidge, K., Burton, C.P., Miner, E.W., Haynes, K.A., Santos, D.F.S., Williams, S.P., Heaton, N., Ingraham, C.M., Lloyd, C., Garceau, D., O'Rourke, R., Herrick, S., Rangel-Barajas, C., Maharjan, S., Wang, N., Sasner, M., Lamb, B.T., Territo, P.R., Sukoff Rizzo, S.J., Carter, G.W., Howell, G.R., Oblak, A.L., 2024. Characterizing molecular and synaptic signatures in mouse models of late-onset Alzheimer's disease independent of amyloid and tau pathology. Alzheimers Dement. 20, 4126–4146.
Lama, A., Pirozzi, C., Severi, I., Morgese, M.G., Senzacqua, M., Annunziata, C., Comella, F., Del Piano, F., Schiavone, S., Petrosino, S., Mollica, M.P., Diano, S., Trabace, L., Calignano, A., Giordano, A., Mattace Raso, G., Meli, R., 2022. Palmitoylethanolamide dampens neuroinflammation and anxiety-like behavior in obese mice. Brain Behav. Immun. 102, 110–123.
Le Thuc, O., Garcia-Caceres, C., 2024. Obesity-induced inflammation: connecting the periphery to the brain. Nat. Metab. 6, 1237–1252.
Li, J., Sun, N., Hu, S., Zuo, Z., 2025. Chronic high fat diet-induced cerebrovascular remodeling impairs recovery of blood flow after cerebral ischemia in mice. J. Cereb. Blood Flow Metab. 45, 1116–1129.
Lohkamp, K.J., van den Hoek, A.M., Solé-Guardia, G., Lisovets, M., Alves Hoffmann, T., Velanaki, K., Geenen, B., Verweij, V., Morrison, M.C., Kleemann, R., Wiesmann, M., Kiliaan, A.J., 2023. The preventive effect of exercise and oral branched-chain amino acid supplementation on obesity-induced brain changes in Ldlr-/-.Leiden mice. Nutrients 15.
Low, A., Mak, E., Malpetti, M., Passamonti, L., Nicastro, N., Stefaniak, J.D., Savulich, G., Chouliaras, L., Su, L., Rowe, J.B., Markus, H.S., O'Brien, J.T., 2020. In vivo neuroinflammation and cerebral small vessel disease in mild cognitive impairment and Alzheimer's disease. J. Neurol. Neurosurg. Psychiatry 92, 45–52.
Lucas, S.J., Cotter, J.D., Brassard, P., Bailey, D.M., 2015. High-intensity interval exercise and cerebrovascular health: curiosity, cause, and consequence. J. Cereb. Blood Flow Metab. 35, 902–911.
Lv, R., Liu, B., Jiang, Z., Zhou, R., Liu, X., Lu, T., Bao, Y., Huang, C., Zou, G., Zhang, Z., Lu, L., Yin, Q., 2025. Intermittent fasting and neurodegenerative diseases: Molecular mechanisms and therapeutic potential. Metabolism 164, 156104.
Mahalakshmi, B., Maurya, N., Lee, S.D., Bharath Kumar, V., 2020. Possible neuroprotective mechanisms of physical exercise in neurodegeneration. Int. J. Mol. Sci. 21.
Maillard, P., Carmichael, O., Harvey, D., Fletcher, E., Reed, B., Mungas, D., DeCarli, C., 2013. FLAIR and diffusion MRI signals are independent predictors of white matter hyperintensities. AJNR Am. J. Neuroradiol. 34, 54–61.
Marini, S., Merino, J., Montgomery, B.E., Malik, R., Sudlow, C.L., Dichgans, M., Florez, J. C., Rosand, J., Gill, D., Anderson, C.D., International Stroke Genetics, C., 2020. Mendelian randomization study of obesity and cerebrovascular disease. Ann. Neurol. 87, 516–524.
Martin, S.S., Aday, A.W., Almarzooq, Z.I., Anderson, C.A.M., Arora, P., Avery, C.L., Baker-Smith, C.M., Barone Gibbs, B., Beaton, A.Z., Boehme, A.K., Commodore-Mensah, Y., Currie, M.E., Elkind, M.S.V., Evenson, K.R., Generoso, G., Heard, D.G., Hiremath, S., Johansen, M.C., Kalani, R., Kazi, D.S., Ko, D., Liu, J., Magnani, J.W., Michos, E.D., Mussolino, M.E., Navaneethan, S.D., Parikh, N.I., Perman, S.M., Poudel, R., Rezk-Hanna, M., Roth, G.A., Shah, N.S., St-Onge, M.P., Thacker, E.L., Tsao, C.W., Urbut, S.M., Van Spall, H.G.C., Voeks, J.H., Wang, N.Y., Wong, N.D., Wong, S.S., Yaffe, K., Palaniappan, L.P., American Heart Association Council on, E., Prevention Statistics, C., Stroke Statistics, S, 2024. 2024 Heart Disease and Stroke Statistics: A Report of US and Global Data From the American Heart Association. Circulation 149, e347–e913.
Masi, S., Ambrosini, S., Mohammed, S.A., Sciarretta, S., Luscher, T.F., Paneni, F., Costantino, S., 2021. Epigenetic remodeling in obesity-related vascular disease. Antioxid. Redox Signal. 34, 1165–1199.
Mielke, M.M., Evans, J.K., Neiberg, R.H., Molina-Henry, D.P., Marcovina, S.M., Johnson, K.C., Carmichael, O.T., Rapp, S.R., Sachs, B.C., Ding, J., Shappell, H.M., Luchsinger, J.A., Espeland, M.A., Hayden, K.M., 2025. Alzheimer disease blood biomarkers and cognition among individuals with diabetes and overweight or obesity. JAMA Netw. Open 8, e2458149.
Miwa, H., Kajimoto, Y., Nakanishi, I., Morita, S., Komoto, J., Kihira, T., Kondo, T., 2003. T2-low signal intensity in the cortex in multiple system atrophy. J. Neurol. Sci. 211, 85–88.
Mollink, J., Hiemstra, M., Miller, K.L., Huszar, I.N., Jenkinson, M., Raaphorst, J., Wiesmann, M., Ansorge, O., Pallebage-Gamarallage, M., van Cappellen van Walsum, A.M., 2019. White matter changes in the perforant path area in patients with amyotrophic lateral sclerosis. Neuropathol. Appl. Neurobiol. 45, 570–585.
Mollink, J., Kleinnijenhuis, M., Cappellen van Walsum, A.V., Sotiropoulos, S.N., Cottaar, M., Mirfin, C., Heinrich, M.P., Jenkinson, M., Pallebage-Gamarallage, M., Ansorge, O., Jbabdi, S., Miller, K.L., 2017. Evaluating fibre orientation dispersion in white matter: comparison of diffusion MRI, histology and polarized light imaging. Neuroimage 157, 561–574.
Montal, V., Vilaplana, E., Alcolea, D., Pegueroles, J., Pasternak, O., Gonzalez-Ortiz, S., Clarimon, J., Carmona-Iragui, M., Illan-Gala, I., Morenas-Rodriguez, E., Ribosa-Nogue, R., Sala, I., Sanchez-Saudinos, M.B., Garcia-Sebastian, M., Villanua, J., Izagirre, A., Estanga, A., Ecay-Torres, M., Iriondo, A., Clerigue, M., Tainta, M., Pozueta, A., Gonzalez, A., Martinez-Heras, E., Llufriu, S., Blesa, R., Sanchez-Juan, P., Martinez-Lage, P., Lleo, A., Fortea, J., 2018. Cortical microstructural changes along the Alzheimer's disease continuum. Alzheimers Dement. 14, 340–351.
Morrison, M.C., Kleemann, R., van Koppen, A., Hanemaaijer, R., Verschuren, L., 2018. Key inflammatory processes in human NASH are reflected in Ldlr(-/-).Leiden mice: a translational gene profiling study. Front. Physiol. 9, 132.
Muoio, V., Persson, P.B., Sendeski, M.M., 2014. The neurovascular unit - concept review. Acta Physiol (Oxf.) 210, 790–798.
Obadia, N., Andrade, G., Leardini-Tristao, M., Albuquerque, L., Garcia, C., Lima, F., Daleprane, J., Castro-Faria-Neto, H.C., Tibirica, E., Estato, V., 2022. TLR4 mutation protects neurovascular function and cognitive decline in high-fat diet-fed mice. J. Neuroinflammation 19, 104.
Olga, L., Bobeldijk-Pastorova, I., Bas, R.C., Seidel, F., Snowden, S.G., Furse, S., Ong, K.K., Kleemann, R., Koulman, A., 2022. Lipid profiling analyses from mouse models and human infants. STAR Protoc. 3, 101679.
Olsson, B., Lautner, R., Andreasson, U., Ohrfelt, A., Portelius, E., Bjerke, M., Holtta, M., Rosen, C., Olsson, C., Strobel, G., Wu, E., Dakin, K., Petzold, M., Blennow, K., Zetterberg, H., 2016. CSF and blood biomarkers for the diagnosis of Alzheimer's disease: a systematic review and meta-analysis. Lancet Neurol. 15, 673–684.
Paiva, I.H.R., Maciel, L.M., Silva, R.S.D., Mendonca, I.P., Souza, J.R.B., Peixoto, C.A., 2024. Prebiotics modulate the microbiota-gut-brain axis and ameliorate anxiety and depression-like behavior in HFD-fed mice. Food Res. Int. 182, 114153.
Park, J.Y., Park, H.J., Kim, D.J., Kim, J.J., 2014. Positive symptoms and water diffusivity of the prefrontal and temporal cortices in schizophrenia patients: a pilot study. Psychiatry Res. 224, 49–57.
Percie du Sert, N., Hurst, V., Ahluwalia, A., Alam, S., Avey, M.T., Baker, M., Browne, W. J., Clark, A., Cuthill, I.C., Dirnagl, U., Emerson, M., Garner, P., Holgate, S.T., Howells, D.W., Karp, N.A., Lazic, S.E., Lidster, K., MacCallum, C.J., Macleod, M., Pearl, E.J., Petersen, O.H., Rawle, F., Reynolds, P., Rooney, K., Sena, E.S., Silberberg, S.D., Steckler, T., Wurbel, H., 2020. The ARRIVE guidelines 2.0: Updated guidelines for reporting animal research. J. Cereb. Blood Flow Metab. 40, 1769–1777.
Prat, A., Biernacki, K., Wosik, K., Antel, J.P., 2001. Glial cell influence on the human blood-brain barrier. Glia 36, 145–155.
Qin, J., Wang, X., Fan, G., Zhang, W., Wu, X., Wang, B., Liu, Y., 2024. Identifying amyotrophic lateral sclerosis using diffusion tensor imaging, and correlation with neurofilament markers. Sci. Rep. 14, 28110.
Richardson, J.P., 1993. Transcription termination. Crit. Rev. Biochem. Mol. Biol. 28, 1–30.
Roitbak, T., Sykova, E., 1999. Diffusion barriers evoked in the rat cortex by reactive astrogliosis. Glia 28, 40–48.
Rong, X., Wei, F., Jiang, Y., Ma, Q., Wang, D., Shen, J., 2025. Microglial activation and hypothalamic structural plasticity in HFD obesity: insights from semaglutide and minocycline. J. Lipid Res. 66, 100736.
Schindelin, J., Arganda-Carreras, I., Frise, E., Kaynig, V., Longair, M., Pietzsch, T., Preibisch, S., Rueden, C., Saalfeld, S., Schmid, B., Tinevez, J.Y., White, D.J., Hartenstein, V., Eliceiri, K., Tomancak, P., Cardona, A., 2012. Fiji: an open-source platform for biological-image analysis. Nat. Methods 9, 676–682.
Schultz, S.A., Strain, J.F., Adedokun, A., Wang, Q., Preische, O., Kuhle, J., Flores, S., Keefe, S., Dincer, A., Ances, B.M., Berman, S.B., Brickman, A.M., Cash, D.M., Chhatwal, J., Cruchaga, C., Ewers, M., Fox, N.N., Ghetti, B., Goate, A., Graff-Radford, N.R., Hassenstab, J.J., Hornbeck, R., Jack Jr., C., Johnson, K., Joseph-Mathurin, N., Karch, C.M., Koeppe, R.A., Lee, A.K.W., Levin, J., Masters, C., McDade, E., Perrin, R.J., Rowe, C.C., Salloway, S., Saykin, A.J., Sperling, R., Su, Y.,

Villemagne, V.L., Voglein, J., Weiner, M., Xiong, C., Fagan, A.M., Morris, J.C., Bateman, R.J., Benzinger, T.L.S., Jucker, M., Gordon, B.A., Dominantly Inherited Alzheimer, N., 2020. Serum neurofilament light chain levels are associated with white matter integrity in autosomal dominant Alzheimer's disease. Neurobiol. Dis. 142, 104960.
Seguella, L., Corpetti, C., Lu, J., Pesce, M., Franzin, S.B., Palenca, I., Zilli, A., Vincenzi, M., Caprioli, D., Paytuvi-Gallart, A., Sanseverino, W., Rurgo, S., Sarnelli, G., Esposito, G., 2025. Oleoylethanolamide-producing Lactobacillus paracasei F19 improves metabolic and behavioral disorders by restoring intestinal permeability and microbiota-gut-brain axis in high-fat diet-induced obese male mice. Brain Behav. Immun. 127, 25–44.
Seidel, F., Fluiter, K., Kleemann, R., Worms, N., van Nieuwkoop, A., Caspers, M.P.M., Grigoriadis, N., Kiliaan, A.J., Baas, F., Michailidou, I., Morrison, M.C., 2023. Ldlr-/-.Leiden mice develop neurodegeneration, age-dependent astrogliosis and obesity-induced changes in microglia immunophenotype which are partly reversed by complement component 5 neutralizing antibody. Front. Cell. Neurosci. 17, 1205261.
Seidel, F., Kleemann, R., van Duyvenvoorde, W., van Trigt;, N., Keijzer, N., van der Kooij, S., van Kooten, C., Verschuren, L., Menke, A., Kiliaan, A.J., Winter, J., Hughes, T.R., Morgan, B.P., Baas, F., Fluiter, K., Morrison, M.C., 2022. Therapeutic intervention with anti-complement component 5 antibody does not reduce NASH but does attenuate atherosclerosis and MIF concentrations in Ldlr-/-.Leiden mice. Int. J. Mol. Sci. 23.
Seidel, F., Morrison, M.C., Arnoldussen, I., Verweij, V., Attema, J., de Ruiter, C., van Duyvenvoorde, W., Snabel, J., Geenen, B., Franco, A., Wiesmann, M., Kleemann, R., Kiliaan, A.J., 2025. Obesity accelerates age-related memory deficits and alters white matter tract integrity in Ldlr-/-.Leiden mice. BBI - Health 45, 100991.
Solé-Guardia, G., Luijten, M., Janssen, E., Visch, R., Geenen, B., Kusters, B., Claassen, J., Litjens, G., de Leeuw, F.E., Wiesmann, M., Kiliaan, A.J., 2025. Deep learning-based segmentation in MRI-(immuno)histological examination of myelin and axonal damage in normal-appearing white matter and white matter hyperintensities. Brain Pathol. 35, e13301.
Song, S.K., Yoshino, J., Le, T.Q., Lin, S.J., Sun, S.W., Cross, A.H., Armstrong, R.C., 2005. Demyelination increases radial diffusivity in corpus callosum of mouse brain. Neuroimage 26, 132–140.
Tanaka, H., Gourley, D.D., Dekhtyar, M., Haley, A.P., 2020. Cognition, brain structure, and brain function in individuals with obesity and related disorders. Curr. Obes. Rep. 9, 544–549.
Tarantini, S., Valcarcel-Ares, M.N., Yabluchanskiy, A., Tucsek, Z., Hertelendy, P., Kiss, T., Gautam, T., Zhang, X.A., Sonntag, W.E., de Cabo, R., Farkas, E., Elliott, M.H., Kinter, M.T., Deak, F., Ungvari, Z., Csiszar, A., 2018. Nrf2 deficiency exacerbates obesity-induced oxidative stress, neurovascular dysfunction, blood-brain barrier disruption, neuroinflammation, amyloidogenic gene expression, and cognitive decline in mice, mimicking the aging phenotype. J. Gerontol. A Biol. Sci. Med. Sci. 73, 853–863.
Tornavaca, O., Chia, M., Dufton, N., Almagro, L.O., Conway, D.E., Randi, A.M., Schwartz, M.A., Matter, K., Balda, M.S., 2015. ZO-1 controls endothelial adherens junctions, cell-cell tension, angiogenesis, and barrier formation. J. Cell Biol. 208, 821–838.
Tucsek, Z., Toth, P., Tarantini, S., Sosnowska, D., Gautam, T., Warrington, J.P., Giles, C. B., Wren, J.D., Koller, A., Ballabh, P., Sonntag, W.E., Ungvari, Z., Csiszar, A., 2014. Aging exacerbates obesity-induced cerebromicrovascular rarefaction, neurovascular uncoupling, and cognitive decline in mice. J. Gerontol. A Biol. Sci. Med. Sci. 69, 1339–1352.
van den Hoek, A.M., Verschuren, L., Worms, N., van Nieuwkoop, A., de Ruiter, C., Attema, J., Menke, A.L., Caspers, M.P.M., Radhakrishnan, S., Salic, K., Kleemann, R., 2020. A translational mouse model for NASH with advanced fibrosis and atherosclerosis expressing key pathways of human pathology. Cells 9.
Vidal-Itriago, A., Radford, R.A.W., Aramideh, J.A., Maurel, C., Scherer, N.M., Don, E.K., Lee, A., Chung, R.S., Graeber, M.B., Morsch, M., 2022. Microglia morphophysiological diversity and its implications for the CNS. Front. Immunol. 13, 997786.
Vilaplana, E., Rodriguez-Vieitez, E., Ferreira, D., Montal, V., Almkvist, O., Wall, A., Lleo, A., Westman, E., Graff, C., Fortea, J., Nordberg, A., 2020. Cortical microstructural correlates of astrocytosis in autosomal-dominant Alzheimer disease. Neurology 94, e2026–e2036.
Waller, R., Baxter, L., Fillingham, D.J., Coelho, S., Pozo, J.M., Mozumder, M., Frangi, A. F., Ince, P.G., Simpson, J.E., Highley, J.R., 2019. Iba-1-/CD68+ microglia are a prominent feature of age-associated deep subcortical white matter lesions. PLoS One 14, e0210888.
Wang, Y.L., Han, Q.Q., Gong, W.Q., Pan, D.H., Wang, L.Z., Hu, W., Yang, M., Li, B., Yu, J., Liu, Q., 2018. Microglial activation mediates chronic mild stress-induced depressive- and anxiety-like behavior in adult rats. J. Neuroinflammation 15, 21.
Wiesmann, M., Zinnhardt, B., Reinhardt, D., Eligehausen, S., Wachsmuth, L., Hermann, S., Dederen, P.J., Hellwich, M., Kuhlmann, M.T., Broersen, L.M., Heerschap, A., Jacobs, A.H., Kiliaan, A.J., 2017. A specific dietary intervention to restore brain structure and function after ischemic stroke. Theranostics 7, 493–512.
Winkler, E.A., Nishida, Y., Sagare, A.P., Rege, S.V., Bell, R.D., Perlmutter, D., Sengillo, J. D., Hillman, S., Kong, P., Nelson, A.R., Sullivan, J.S., Zhao, Z., Meiselman, H.J., Wendy, R.B., Soto, J., Abel, E.D., Makshanoff, J., Zuniga, E., De Vivo, D.C., Zlokovic, B.V., 2015. GLUT1 reductions exacerbate Alzheimer's disease vasculo-neuronal dysfunction and degeneration. Nat. Neurosci. 18, 521–530.
Wittekindt, M., Kaddatz, H., Joost, S., Staffeld, A., Bitar, Y., Kipp, M., Frintrop, L., 2022. Different methods for evaluating microglial activation using anti-ionized calcium-binding adaptor protein-1 immunohistochemistry in the cuprizone model. Cells 11.
Worrall, B.B., Thohan, C.S., 2024. Factor XI as the possible underlying mechanism between stroke and obesity. Neurology 103, e209616.
Wu, M., Liao, M., Huang, R., Chen, C., Tian, T., Wang, H., Li, J., Li, J., Sun, Y., Wu, C., Li, Q., Xiao, X., 2022. Hippocampal overexpression of TREM2 ameliorates high fat diet induced cognitive impairment and modulates phenotypic polarization of the microglia. Genes Dis 9, 401–414.
Yi, C.X., Gericke, M., Kruger, M., Alkemade, A., Kabra, D.G., Hanske, S., Filosa, J., Pfluger, P., Bingham, N., Woods, S.C., Herman, J., Kalsbeek, A., Baumann, M., Lang, R., Stern, J.E., Bechmann, I., Tschop, M.H., 2012. High calorie diet triggers hypothalamic angiopathy. Mol. Metab. 1, 95–100.
Zerbi, V., Kleinnijenhuis, M., Fang, X., Jansen, D., Veltien, A., Van Asten, J., Timmer, N., Dederen, P.J., Kiliaan, A.J., Heerschap, A., 2013. Gray and white matter degeneration revealed by diffusion in an Alzheimer mouse model. Neurobiol. Aging 34, 1440–1450.
Zhang, S.S., Zhu, L., Peng, Y., Zhang, L., Chao, F.L., Jiang, L., Xiao, Q., Liang, X., Tang, J., Yang, H., He, Q., Guo, Y.J., Zhou, C.N., Tang, Y., 2022. Long-term running exercise improves cognitive function and promotes microglial glucose metabolism and morphological plasticity in the hippocampus of APP/PS1 mice. J. Neuroinflammation 19, 34.

Xiaoxue Liang Department of Medical Imaging, Anatomy, Research Institute for Medical Innovation, Radboud University Medical Center, Donders Institute for Brain, Cognition and Behavior, Center for Medical Neuroscience, Radboud Technology Center Preclinical imaging PRIME, Radboud Alzheimer Center, Nijmegen, the Netherlands. Address: Radboud university medical center, Department of Medical Imaging, Anatomy (109), PO Box 9101, 6525 EZ Nijmegen, the Netherlands. Email: Xiaoxue.Liang@radboudumc.nl.

Klara J. Lohkamp Department of Medical Imaging, Anatomy, Research Institute for Medical Innovation, Radboud University Medical Center, Donders Institute for Brain, Cognition and Behavior, Center for Medical Neuroscience, Radboud Technology Center Preclinical imaging PRIME, Radboud Alzheimer Center, Nijmegen, the Netherlands. Address: Radboud university medical center, Department of Medical Imaging, Anatomy (109), PO Box 9101, 6525 EZ Nijmegen, the Netherlands. Email: Klara.Lohkamp@radboudumc.nl.

Dr. Anita M. van den Hoek Department of Metabolic Health Research, The Netherlands Organization for Applied Scientific Research (TNO), Leiden, the Netherlands. Address: TNO – Location Leiden – Sylviusweg, Sylviusweg 71, 2333 BE Leiden, the Netherlands. Email: a.vandenhoek@tno.nl.

Bram Geenen Department of Medical Imaging, Anatomy, Research Institute for Medical Innovation, Radboud University Medical Center, Donders Institute for Brain, Cognition and Behavior, Center for Medical Neuroscience, Radboud Technology Center Preclinical imaging PRIME, Radboud Alzheimer Center, Nijmegen, the Netherlands. Address: Radboud university medical center, Department of Medical Imaging, Anatomy (109), PO Box 9101, 6525 EZ Nijmegen, the Netherlands. Email: Bram.Geenen@radboudumc.nl.

Vivienne Verweij Department of Medical Imaging, Anatomy, Research Institute for Medical Innovation, Radboud University Medical Center, Donders Institute for Brain, Cognition and Behavior, Center for Medical Neuroscience, Radboud Technology Center Preclinical imaging PRIME, Radboud Alzheimer Center, Nijmegen, the Netherlands. Address: Radboud university medical center, Department of Medical Imaging, Anatomy (109), PO Box 9101, 6525 EZ Nijmegen, the Netherlands. Email: Vivienne.Verweij@radboudumc.nl.

Dr. Martine C. Morrison, Department of Metabolic Health Research, The Netherlands Organization for Applied Scientific Research (TNO), Leiden, the Netherlands. Address: TNO – Location Leiden – Sylviusweg, Sylviusweg 71, 2333 BE Leiden, the Netherlands. Email: Martine.Morrison@tno.nl.

Dr. Robert Kleemann Department of Metabolic Health Research, The Netherlands Organization for Applied Scientific Research (TNO), Leiden, the Netherlands. Address: TNO – Location Leiden – Sylviusweg, Sylviusweg 71, 2333 BE Leiden, the Netherlands. Email: Robert.Kleemann@tno.nl.

Prof. dr. Amanda J Kiliaan (# Corresponding author) Department of Medical Imaging, Anatomy, Research Institute for Medical Innovation, Radboud University Medical Center, Donders Institute for Brain, Cognition and Behavior, Center for Medical Neuroscience, Radboud Technology Center Preclinical imaging PRIME, Radboud Alzheimer Center, Nijmegen, the Netherlands. Address: Radboud university medical center, Department of Medical Imaging, Anatomy (109), PO Box 9101, 6525 EZ Nijmegen, the Netherlands. Phone: +31 24 361 4378 - Fax: +31 24 361 3789. Email: Amanda.Kiliaan@radboudumc.nl.

Dr. Maximilian Wiesmann Department of Medical Imaging, Anatomy, Research Institute for Medical Innovation, Radboud University Medical Center, Donders Institute for Brain, Cognition and Behavior, Center for Medical Neuroscience, Radboud Technology Center Preclinical imaging PRIME, Radboud Alzheimer Center, Nijmegen, the Netherlands. Address: Radboud university medical center, Department of Medical Imaging, Anatomy (109), PO Box 9101, 6525 EZ Nijmegen, the Netherlands. Email: Maximilian.Wiesmann@radboudumc.nl.

Dr. Gemma Solé-Guardia Department of Medical Imaging, Anatomy, Research Institute for Medical Innovation, Radboud University Medical Center, Donders Institute for Brain, Cognition and Behavior, Center for Medical Neuroscience, Radboud Technology Center Preclinical imaging PRIME, Radboud Alzheimer Center, Nijmegen, the Netherlands. Address: Radboud university medical center, Department of Medical Imaging, Anatomy (109), PO Box 9101, 6525 EZ Nijmegen, the Netherlands. Department of Neurology, Research Institute for Medical Innovation, Radboud university medical center, Donders Institute for Brain, Cognition and Behaviour, Centre for medical neuroscience, Nijmegen, the Netherlands. Address: Radboud university medical center, department of Neurology, PO Box 9101, 6500 HB Nijmegen, the Netherlands. Email: Gemma.SoleGuardia@radboudumc.nl.